Asian Journal of Chemistry; Vol. 33, No. 12 (2021), 3006-3024

ASIAN JOURNAL OF CHEMISTRY

https://doi.org/10.14233/ajchem.2021.23408

Synthesis, Characterization and DNA Binding Studies of Some Hydrazide Derivatives Schiff Base Metal Complexes of Mn(II), Co(II/III), Ni(II), Cu(II) and Zn(II) Metal Ions

RAMINA, RAJKUMAR BHUBON SINGH* and OINAM U-WANG

Department of Chemistry, Manipur University, Canchipur-795003, India

*Corresponding author: E-mail: bhubonsingh@gmail.com

Received: 9 July 2021; *Accepted*: 3 September 2021; *Published online*: 6 December 2021; AJC-20593

Eighteen metal complexes were synthesized by using four different Schiff base ligands, (1*E*)-1-((6-methyl-4-oxo-4*H*-chromen-3-yl)methylene)carbohydrazide (**L_1**), 6-[2-(salicylidene)hydrazinyl]-*N*′-(salicylidene)nicotinohydrazide (**HL_2**), 6-hydrazinyl-*N*′-(6-methyl-4-oxo-4*H*-chromen-3-yl-methylene)nicotinohydrazide (**HL_3**) and (*E*)-6-hydrazinyl-*N*′-(1-(2,3-dihydro-1,3-dioxo-1*H*-inden-2-yl)-ethylidene)pyridine-3-carbohydrazide (**L_4**). Characterization of the metal complexes were carried out by using various physico-chemical techniques. Complexes **1**, **3**, **4**, **6**, **11**, **14**, **15**, **16**, **17** and **18** have been found octahedral structures while the metal complexes **2**, **5**, **8**, **10** and **13** have tetrahedral structures. And, complexes **7**, **9** and **12** have square planar structures. Thermal study has revealed the presence of lattice and coordinated water molecules in the complexes. From powder X-ray diffraction study, it was suggested that a monoclinic system for complexes **2** and **14** while a triclinic system for the complexes **3, 4, 5**, **9**, **11**, **13** and **15**. The interaction of the ligands and their metal complexes with calf thymus DNA (CT-DNA) has been studied by electronic absorption, cyclic voltammetry and viscosity methods.

Keywords: Thiocyanato, Schiff base ligands, Metal(II/III) complexes, DNA interaction study.

INTRODUCTION

Design and synthesis of novel hydrazones and their metal complexes are still continuing in this era due to their wide potential applications like antitumor, antimicrobial, antioxidant, antifouling, flame retardant, iron overload treatment, catalytic, analytical, DNA binding and cleavage agents [1-5]. It may be mentioned that starting compound carbohydrazide can facilitate polynuclear hydrazone complexes with a variety of metal ions using the two hydrazine groups in presence of carbonyl compounds [6-10]. Some metal hydrazone complexes of this hydrazide were found to have potential antibacterial, antioxidant, antimicrobial, anti-fungicidal, flame colorants and catalytic properties [11-18]. Some hydrazones obtained using this hydrazide have been reported of employing as Cd(II) and Fe(III) ions as sensors [19,20]. Besides, study on hydrazones containing pyridine ring moiety has been extended from an earlier time due to their capability of using them as analytical reagents [21]. For example, hydrazone derived from 7-methoxychromone-3-carbaldehyde and nicotinic acid hydrazide has been reported to serve as an efficient fluorescent probe for Al^{3+} in ethanol medium [22]. Some hydrazones of isonicotinic and nicotinic acid hydrazides have been encountered to have good antimicrobial, anti-inflammatory, analgesic and antitubercular activities [23-25]. It has been reported that nicotinamido-4-*bis*(2-chloroethyl)aminobenzaldimine (NBAB) and its copper complex possess significant antitumor activities [26].

In DNA binding studies, hydrazone metal complexes have been paid importance as they interact and bind with DNA double helix covalently or non-covalently depending on the nature of ligands, oxidation states and coordination environment [27]. In many DNA targeting drug development processes, it has been found that an intercalative binding mode of small molecules is rather vital than the other non-covalent modes namely groove binding, electrostatic and partial intercalation. Various applications like DNA foot printing, DNA cleaving agents, DNA structural probes, as diagnostic as well as curing agents for various ailments and so on have been reported to develop successfully with the understanding of interaction ways and affinity of the complexes to DNA [28-30]. These features pave the interest to study in the field of chemistry, molecular biology and medicine [31,32].

In consideration of the above findings and to continue our work [33-35] on synthesis, characterization and DNA binding studies of metal complexes, we herein report the synthesis of eighteen Schiff base metal complexes of Mn(II), Co(II/III), Ni(II), Cu(II) and Zn(II) metal ions derived from four different ligands namely (1*E*)-1-((6-methyl-4-oxo-4*H*-chromen-3-yl)-methylene)carbohydrazide (**L_1**), 6-[2-(salicylidene)-hydrazinyl]-*N*′-(salicylidene) nicotinohydrazide (**HL_2**), 6-hydrazinyl-*N*′-(6-methyl-4-oxo-4*H*-chromen-3-yl-methylene)-nicotinohydrazide (**HL_3**) and (*E*)-6-hydrazinyl-*N*′-(1-(2,3-dihydro-1,3-dioxo-1*H*-inden-2-yl)ethylidene)pyridine-3-carbohydrazide (**L_4**), characterization and DNA binding studies of the ligands and their metal complexes by different spectroscopic methods.

EXPERIMENTAL

Carbohydrazide, 6-hydrazino-nicotinic acid hydrazide, 3-formyl-6-methyl-chromone, salicylaldehyde, 2-acetyl-1,3-indane-dione, metal(II) salts, ammonium thiocyanate, sodium azide and solvents were procured from Sigma-Aldrich and Merck, India. CT-DNA and Tris–HCl (biological grade) were procured from Himedia. All chemicals and solvents are used without further purification. Elemental analyses (C, H and N) were carried on a Perkin-Elmer 2400-II elemental analyzer. Infrared spectra were recorded on a Perkin-Elmer FTIR 400 spectrophotometer (KBr pellets, 4000-400 cm^{-1}). UV-Vis spectra were recorded on a Shimadzu UV-visible 2450 spectrophotometer. Magnetic susceptibility at room temperature was measured using Sherwood magnetic susceptibility balance using $CuSO_4 \cdot 5H_2O$ as standard substance. Molar conductivity was performed on a Eutech Con 510 conductometer at 25 ºC in DMSO/DMF (10^{-3} mol L^{-1}). Thermal spectra were recorded on a Perkin-Elmer STA 6000 Simultaneous Thermal Analyzer at a heating rate of 10 ºC per min. ESR spectra were recorded on a X-band, JEOL, JES-FA200 ESR spectrometer (RT and LNT). NMR (^{1}H DMSO-d_6 & ^{13}C solid) spectra were recorded on a FT-NMR Bruker Avance II 400 and FT NMR JEOL ECX-400 spectrometers. Mass spectra were recorded on a Waters UPLC- TQD (ESI-MS) spectrometer. Powder XRD spectra were recorded on a PAN-analytical Philips diffractometer. The effect of ligands and metal complexes on DNA was analyzed by CV using a CH602C electrochemical analyzer ($AgNO_3$/Ag as reference electrode). Viscosity measurement of CT-DNA was performed using an Ostwald's viscometer placed in a thermostat water bath at 298 K. From the equation $\eta = (t\text{-}t_o)/t_o$, η and η_o have been determined. Where, t_o and t are the flow times of buffer alone and CT-DNA solution containing ligands and complexes.

Synthesis of Schiff base ligands

(1*E*)-1-((6-Methyl-4-oxo-4*H*-chromen-3-yl)methylene)-carbohydrazide (L_1): Solutions of carbohydrazide (1 mmol, 0.090 g) (30 mL) and 3-formyl-6-methylchromone (1 mmol, 0.188 g) (20 mL) in methanol were refluxed for 4 h to give an off-white precipitate. It was filtered, washed with the solvent and air dried.

6-[2-(Salicylidene)hydrazinyl]-*N*′-(salicylidene)nicotino-hydrazide (HL_2): Methanolic solutions of 6-hydrazino-nicotinic acid hydrazide hydrate (1 mmol, 0.167 g) (20 mL) and salicylaldehyde (2 mmol, 0.212 mL) (10 mL) were refluxed for 4 h to give a yellow precipitate, filtered, washed with the solvent and air dried.

6-Hydrazinyl-*N*′-(6-methyl-4-oxo-4*H*-chromen-3-yl-methylene)nicotinohydrazide (HL_3): Methanolic solutions of 6-hydrazino-nicotinic acid hydrazide hydrate (1 mmol, 0.167 g) (20 mL) and 3-formyl-6-methyl-chromone (1 mmol, 0.188 g) (20 mL) were refluxed for 4 h to give a yellow precipitate. It was filtered, washed with the solvent and air dried.

(*E*)-6-Hydrazinyl-*N*′-(1-(2,3-dihydro-1,3-dioxo-1*H*-inden-2-yl)ethylidene)pyridine-3-carbohydrazide (L_4): Methanolic solutions of 6-hydrazinonicotinic hydrazide hydrate (1 mmol, 0.167 g) (20 mL) and 2-acetyl-1,3-indanedione (1 mmol, 0.188 g) (20 mL) were refluxed for 4 h to give a yellow precipitate. It was filtered, washed with the solvent and dried in air.

L_1: Yield: 70.11%, off-white, m.p.: 203 ºC, *m.w.*: 260.25, Anal. calcd. (found) % for $C_{12}H_{12}N_4O_3$: C, 55.38 (55.29); H, 4.64 (4.67); N, 21.53 (21.50); IR (KBr, ν_{max}, cm^{-1}): 3211 (N-H), 3036 (Ar-CH), 1689 (C=O) amide(I), 1643 (C=O) chromone, 1627 (C=N), 1535 amide (II); ^{1}H NMR (400 MHz, DMSO-d_6, δ, ppm): 10.80 (s, 1H, CONH), 8.93 (s, 1H, NH), 8.28 (s, 1H, CH=N), 7.59-7.89 (m, 4H, aromatic ring), 3.36 (s, 2H, NH_2), 2.48 (s, 3H, CH_3).

HL_2: Yield: 68.51%, yellow, m.p.: 265 ºC, *m.w.*: 375.39, Anal. calcd. (found) % for $C_{20}H_{17}N_5O_3$: C, 63.99 (64.09); H, 4.56 (4.49); N, 18.66 (18.60); IR (KBr, ν_{max}, cm^{-1}): 3572, 3232 (OH)/(N-H), 3059 (Ar-CH), 1635 (C=O) amide(I), 1606 (C=N), 1537 amide (II), 1201 (C-O); ^{1}H NMR (400 MHz, DMSO-d_6, δ, ppm): 8.35 (s, 1H, NH), 8.40 (s, 2H, C=N), 6.86-8.18 (m, 11H, aromatic ring), 8.61 (s, 1H, CONH), 8.74 (s, 1H, Ar-OH).

HL_3: Yield: 67.23%, yellow, m.p.: 224 ºC, *m.w.*: 337.34, Anal. calcd. (found) % for $C_{17}H_{15}N_5O_3$: C, 60.53 (60.47); H, 4.48 (4.50); N, 20.76 (20.68); IR (KBr, ν_{max}, cm^{-1}): 3444, 3339, 3206 (OH)/(N-H), 1685 (C=O, amide(I)), 1649 (C=O, chromone), 1618 (C=N); ^{13}C NMR (400 MHz, solid, δ, ppm): 176.00, 174.44 (C=O, amide and exo), 133.70 (azomethine carbon), 153.53 (C-O, chromone), 115.14-127.25 (chromone moiety carbons), 158.22, 142.10, 139.07, 136.53, 107.52 (pyridine ring), 22.72 (CH_3).

L_4: Yield: 65.13%, yellow, m.p.: 250 ºC, *m.w.*: 337.34, Anal. calcd. (found) % for $C_{17}H_{15}N_5O_3$: C, 60.53 (60.60); H, 4.48 (4.40); N, 20.76 (20.72); IR (KBr, ν_{max}, cm^{-1}): 3491, 3315, 3217 (OH)/(N-H), 1693 (C=O, amide(I)), 1643 (C=O, *exo*), 1591 (C=N), 1537 amide (II); ^{1}H NMR (400 MHz, DMSO-d_6, δ, ppm): 8.66 (s, 1H, CONH), 6.83-8.07 (m, 8H, aromatic ring), 3.14 (s, 2H, NH_2), 2.48 (s, 3H, CH_3).

Synthesis of metal(II/III) complexes: In the synthetic pathway of the complex **4** or **6**, 2 mmol of ligand **L_1** or **HL_2** was utilized in the 1:2 molar ratio of the metal and ligands. Whereas, the remaining complexes were synthesized in (1:1) molar ratio of the metal and ligands.

Complex 1: To an ethanolic solution of **L_1** (1 mmol, 0.260 g) (30 mL), aqueous solution of $Mn(CH_3COO)_2 \cdot 4H_2O$ (1 mmol, 0.245 g) (10 mL) was added with stirring at room temperature for about 0.5 h. Then solution mixture was conti-nued to reflux

for about 6 h in the presence of aqueous NaOH (4 mmol, 0.160 g) to give the brown precipitate. It was filtered, washed with the solvent and air dried (**Scheme-I**).

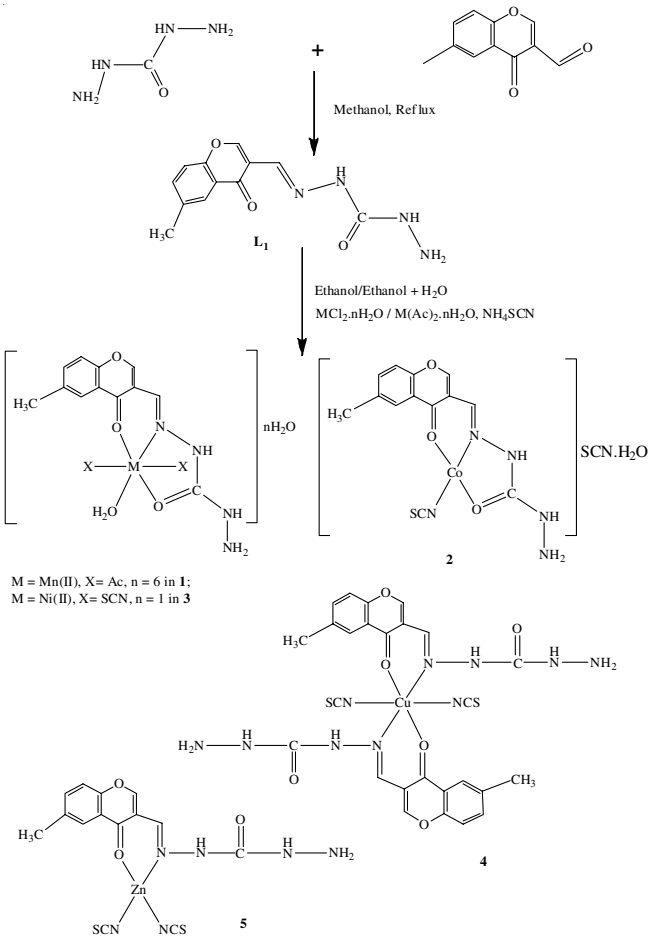

Scheme-I: Reaction scheme of the complexes **1-5**

Complex 2-5: To an ethanolic solution of $\mathbf{L_1}$ (1 mmol, 0.260 g)/(2 mmol, 0.520 g) (30 mL), $CoCl_2{\cdot}6H_2O$ (1 mmol, 0.237 g) (10 mL) (**2**), $NiCl_2.6H_2O$ (1 mmol, 0.237 g) (10 mL) (**3**), $CuCl_2{\cdot}2H_2O$ (1 mmol, 0.170 g) (10 mL) (**4**) and $ZnCl_2$ (1 mmol, 0.199 g) (**5**) (10 mL) metal salts were added in the same medium with stirring at room temperature. After 0.5 h of the stirring, aqueous solution of NH_4SCN (2 mmol, 0.152 g) (10 mL) was added in each and continued for another 0.5 h. Then, solution mixtures were refluxed for about 6 h to give the respective complexes. It was filtered, washed with the solvent and air dried (**Scheme-I**).

Complexes 6-7: To an acetonitrile solution of $\mathbf{HL_2}$ (2 mmol, 0.750 g)/(1 mmol, 0.375 g) (30 mL), $MnCl_2{\cdot}4H_2O$ (1 mmol, 0.196 g) (10 mL) (**6**) and $Co(NO_3)_2{\cdot}6H_2O$ (1 mmol, 0.291 g) (10 mL) (**7**) metal salts in the aqueous medium were added with constant stirring at room temperature for about 1 h. Then solution mixtures were continued to reflux for about 6 h in the presence of triethylamine (2 mmol, 0.2786 g) or aqueous NaOH (2 mmol, 0.080 g) to give corresponding compounds. It was filtered, washed with the solvent and air dried (**Scheme-II**).

Complexes 8-10: To an acetonitrile solution of $\mathbf{HL_2}$ (1 mmol, 0.375 g) (30 mL), $NiCl_2.6H_2O$ (1 mmol, 0.197 g) (10 mL) (**8**),

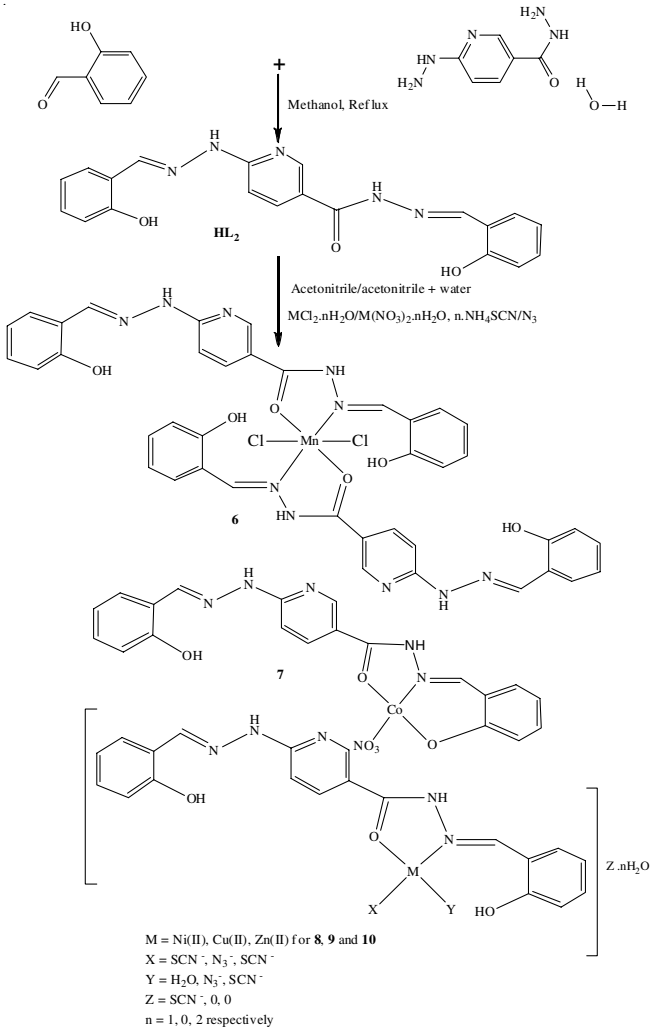

Scheme-II: Reaction scheme of the metal complexes **6-10**

$Cu(NO_3)_2{\cdot}3H_2O$ (1 mmol, 0.241 g) (10 mL) (**9**) and $Zn(NO_3)_2{\cdot}6H_2O$ (1 mmol, 0.297 g) (10 mL) (**10**) metal salts were added separately in the same medium with constant stirring at room temperature. After 0.5 h of the stirring, aqueous solution of NH_4SCN (2 mmol, 0.152 g) (10 mL) was added to the above solution except for complex **9** where aqueous solution of sodium azide (2 mmol, 0.130 g) (10 mL) was used. Stirring was continued for another 0.5 h and the solution was refluxed for about 6 h in the presence of triethylamine (2 mmol, 0.2786 g) or aqueous NaOH (2 mmol, 0.080 g) (**10**) to give the respective compounds. Then filtered, washed with the solvent and air dried (**Scheme-II**).

Complexes 11-15: Acetonitrile solution of $MnCl_2{\cdot}4H_2O$ (1 mmol, 0.197 g) (10 mL) (**11**), $Co(NO_3)_2.6H_2O$ (1 mmol, 0.291 g) (10 mL) (**12**), $NiCl_2.6H_2O$ (1 mmol, 0.237 g) (10 mL) (**13**), $CuCl_2.2H_2O$ (1 mmol, 0.170 g) (10 mL) (**14**) and $ZnCl_2$ (1 mmol, 0.136 g) (10 mL) (**15**) were added to the hot suspension of $\mathbf{HL_3}$ (1 mmol, 0.337 g) (30 mL) in the same medium with constant stirring. After 0.5 h of the stirring, aqueous solution of NH_4SCN (2 mmol, 0.152 g) (10 mL) was added to the respective solutions except for complex **14** and continue for another 0.5 h. Then, solution mixtures were refluxed for about 6 h to give the respective coloured compounds (**Scheme-III**).

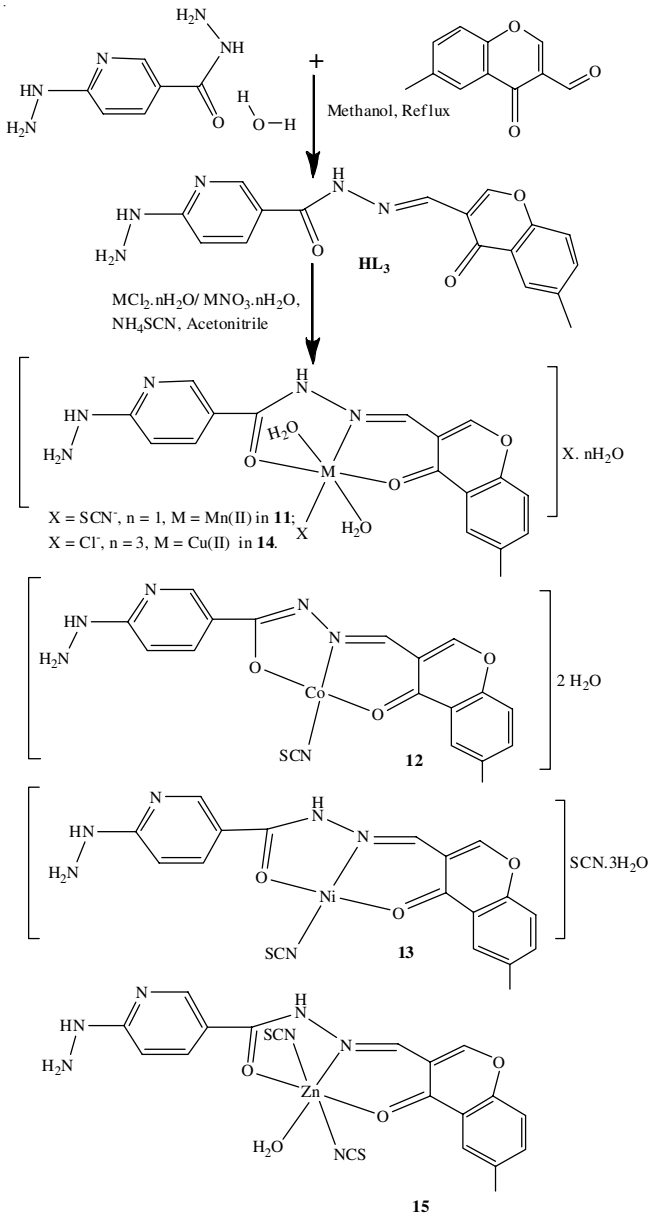

Scheme-III: Reaction scheme of the metal complexes **11**-**15**

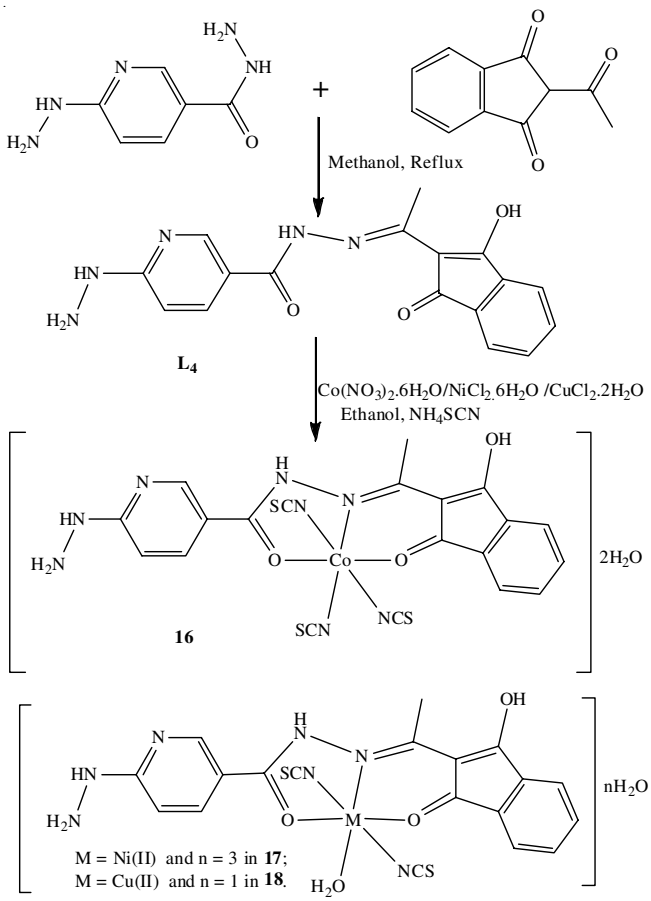

Scheme-IV: Reaction scheme of the metal complexes **16**-**18**

Complexes 16-18: To an ethanolic solution of $\mathbf{L_4}$ (1 mmol, 0.337 g) (30 mL), $Co(NO_3)_2{\cdot}6H_2O$ (1 mmol, 0.291 g) (10 mL) (**16**), $NiCl_2.6H_2O$ (1 mmol, 0.237 g) (10 mL) (**17**) and $CuCl_2{\cdot}2H_2O$ (1 mmol, 0.170 g) (10 mL) (**18**) metal salts in the same medium were added with constant stirring at room temperature. After 0.5 h of the stirring, aqueous solution of NH_4SCN (3 mmol, 0.228 g) in complex **16** or (2 mmol, 0.152 g) in complexes **17** and **18** (10 mL) was added and continued for another 0.5 h. Then, solution mixtures were refluxed for about 6 h to give the corresponding metal complexes (**Scheme-IV**).

$[Mn(L_1)(OAc)_2(H_2O)]{\cdot}6H_2O$ (1): Yield: 70.51%, brown, m.p.: > 300 ºC, *m.w.*: 559.38, Anal. calcd. (found) % for $C_{16}H_{32}N_4O_{14}Mn$: C, 34.36 (34.40); H, 5.76 (5.69); N, 10.02 (10.10); IR (KBr, ν_{max}, cm^{-1}): 3394(br) (OH)/(N-H), 1664 (C=O) amide(I), 1629 (C=O) chromone, 1580 (C=N), 1514 amide (II), 468 (M-O), 439 (M-N), 1629, 1344 (asymmetric and symmetric stretching vibrations for acetate group in monodentate mode); UV-Vis (λ_{max}) (DMSO): 30,120 cm^{-1} [$^6A_{1g}$ (S) → ^4E_g (D)] octahedral; molar conductance (DMSO): 2.26 Ω^{-1} cm^2 mol^{-1}; μ_{eff} (B.M.): 5.21.

$[Co(L_1)(NCS)]NCS.H_2O$ (2): Yield: 60.71%, green, m.p.: 240 ºC, *m.w.*: 453.37, Anal. calcd. (found) % for $C_{14}H_{14}N_6O_4S_2Co$: C, 37.09 (36.96); H, 3.11 (3.12); N, 18.54 (18.50); IR (KBr, ν_{max}, cm^{-1}): 3325, 3186 (OH)/(N-H), 3043 (CH)aryl, 1666 (C=O) amide(I), 1639 ν(C=O) chromone, 1620 (C=N), 1573 amide (II), 2096 (M-NCS, terminal), 472 ∂(NCS), 601 (M-O), 435 (M-N); UV-Vis (λ_{max}) (DMSO): 13,333 cm^{-1} [$^4A_2$ (F) → $^4T_1$ (P) (ν_3)] tetrahedral; ESI-MS (*m/z* value for M^+): 453; molar conductance (DMSO): 37.55 Ω^{-1} cm^2 mol^{-1}; μ_{eff} (B.M.): 4.06.

$[Ni(L_1)(NCS)_2(H_2O)]H_2O$ (3): Yield: 62.51%, green, m.p.: > 300 ºC, *m.w.*: 471.14, Anal. calcd. (found) % for $C_{14}H_{16}N_6O_5S_2Ni$: C, 35.69 (35.62); H, 3.42 (3.38); N, 17.83 (17.89); IR (KBr, ν_{max}, cm^{-1}): 3599, 3292 (OH)/(N-H), 3043 (CH)aryl, 1635 (C=O) amide(I), 1604 ν(C=O) chromone, 1589 (C=N), 1577 amide (II), 2092 (M-NCS, terminal), 470 δ(NCS), 615 (M-O), 430 (M-N); UV-Vis (λ_{max}) (DMSO): 13,106, 16,207, 26,737 cm^{-1} [$^3A_{2g}(F) \rightarrow {}^3T_{2g}(F)$ (ν_1), $^3A_{2g}(F) \rightarrow {}^3T_{1g}(F)$ (ν_2), $^3A_{2g}(F) \rightarrow {}^3T_{1g}(P)$ (ν_3)] octahedral; ESI-MS (*m/z* value for M^+): 470; molar conductance (DMSO): 16.26 Ω^{-1} cm^2 mol^{-1}; μ_{eff} (B.M.): 2.88.

$[Cu(L_1)_2(\mu\text{-}NCS)_2]$ (4): Yield: 67.41%, yellow, m.p.: 240 ºC, *m.w.*: 700.22, Anal. calcd. (found) % for $C_{26}H_{24}N_{10}O_6S_2Cu$: C, 44.60 (44.66); H, 3.45 (3.38); N, 20.00 (20.14); IR (KBr, ν_{max}, cm^{-1}): 3234 (N-H), 3041 (CH)aryl, 1691 (C=O) amide(I),

1639 (C=O) chromone, 1548 (C=N)/amide (II), 2117 (M-NCS, bridging), 464 δ(NCS), 615 (M-O), 426 (M-N); UV-Vis (λ_{max}) (DMSO): 14,534 cm^{-1} ($^2B_{1g} \rightarrow {}^2A_{1g}$) distorted octahedral; ESI-MS (*m/z* value for M^+): 700; molar conductance (DMSO): 16.85 Ω^{-1} cm^2 mol^{-1}; μ_{eff} (B.M.): 1.37.

$[Zn(L_1)(NCS)_2]$ (5): Yield: 69.71%, yellow, m.p.: 210 ºC, *m.w.*: 441.80, Anal. calcd. (found) (%) for $C_{14}H_{12}N_6O_3S_2Zn$: C, 38.06 (38.12); H, 2.74 (2.70); N, 19.02 (19.07); IR (KBr, ν_{max}, cm^{-1}): 3242, 3169 (N-H), 3061 (CH)aryl, 1691 (C=O) amide(I), 1631 (C=O) chromone, 1618 (C=N), 1550 amide (II), 2081 (M-NCS, terminal), 470 δ(NCS), 605 (M-O), 443 (M-N); ^{13}C NMR (400 MHz, solid, δ, ppm): 176 (C=O) (amide and exo), 166 (azomethine carbon), 153.63 (C-O, chromone), 112.79-146 (chromone moiety carbons), 21.65 (CH_3); ESI-MS (*m/z* value for M^+): 441; molar conductance (DMSO): 14.39 Ω^{-1} cm^2 mol^{-1}; μ_{eff} (B.M.): diamagnetic.

$[Mn(HL_2)_2(Cl)_2]$ (6): Yield: 67.41%, yellow, m.p.: 290 ºC, *m.w.*: 876.62, Anal. calcd. (found) (%) for $C_{40}H_{34}N_{10}O_6Cl_2Mn$: C, 54.81 (54.76); H, 3.91 (3.95); N, 15.98 (16.02); IR (KBr, ν_{max}, cm^{-1}): 3587, 3221 (OH)/(N-H), 3055 (CH)aryl, 1604 (C=O) amide(I), 1604 (C=N), 1533 amide (II), 1201 (C-O), 441 (M-O), 403 (M-N); UV-Vis (λ_{max}) (DMSO): 22,935 cm^{-1} [$^6A_{1g} \rightarrow {}^4E_g$, $^4A_{1g}$ (G)] octahedral; ESI-MS (*m/z* value for M^+): 876; molar conductance (DMSO): 1.46 Ω^{-1} cm^2 mol^{-1}; μ_{eff} (B.M.): 4.13.

$[Co(L_2)(NO_3)]$ (7): Yield: 69.81%, brown, m.p.: > 300 ºC, *m.w.*: 495.32, Anal. calcd. (found) (%) for $C_{20}H_{16}N_6O_6Co$: C, 48.450 (48.41); H, 3.26 (3.20); N, 16.97 (17.00); IR (KBr, ν_{max}, cm^{-1}): 3431(br) (OH)/(N-H), 1622 (C=O) amide(I), 1597 (C=N), 1541 amide (II), 1444, 1305 (ν_5 and ν_1 stretching vibrations of monodentate nitrate group), 1247 (C-O), 516 (M-O), 484 (M-N); UV-Vis (λ_{max}) (DMSO): 22,624 cm^{-1} ($A_{1g} \rightarrow B_{1g}$) square planar; ESI-MS (*m/z* value for M^+): 495.28; molar conductance (DMF): 52.91 Ω^{-1} cm^2 mol^{-1}; μ_{eff} (B.M.): 2.84.

$[Ni(HL_2)(NCS)(H_2O)](NCS)\cdot H_2O$ (8): Yield: 69.81%, yellowish-green, m.p.: > 300 ºC, *m.w.*: 586.28, Anal. calcd. (found) (%) for $C_{22}H_{21}N_7O_5S_2Ni$: C, 45.07 (45.10); H, 3.61 (3.58); N, 16.72 (16.68); IR (KBr, ν_{max}, cm^{-1}): 3564, 3174 (OH)/(N-H), 3063 (CH)aryl, 1620 (C=O) amide(I), 1620 (C=N), 1523 amide (II), 2106 (M-NCS, terminal), 1197 (C-O), 516 (M-O), 428 (M-N); UV-Vis (λ_{max}) (DMSO): 13,262 cm^{-1} [$^3T_1(F) \rightarrow {}^3T_1(P)$ (ν_3)] distorted tetrahedral; ESI-MS (*m/z* value for M^+): 585; molar conductance (DMSO): 47.80 Ω^{-1} cm^2 mol^{-1}; μ_{eff} (B.M.): 2.85.

$[Cu(HL_2)(N_3)_2]$ (9): Yield: 71.51%, green, m.p.: > 300 ºC, *m.w.*: 523.12, Anal. calcd. (found) (%) for $C_{20}H_{17}N_{11}O_3Cu$: C, 45.92 (63.81); H, 3.28 (3.31); N, 29.45 (29.50); IR (KBr, ν_{max}, cm^{-1}): 3585, 3196 (OH)/(N-H), 3061 (CH)aryl, 1620 (C=O) amide(I), 1620 (C=N), 1535 amide (II), 2063 (asymmetric M-N_3 terminal), 1201 (C-O), 501 (M-O), 424 (M-N); UV-Vis (λ_{max}) (DMSO): 15,772 cm^{-1} ($^2B_{1g} \rightarrow {}^2A_{1g}$) square planar; ESI-MS (*m/z* value for M^+): 522; molar conductance (DMSO): 17.06 Ω^{-1} cm^2 mol^{-1}; μ_{eff} (B.M.): 1.71.

$[Zn(HL_2)(NCS)_2]\cdot 2H_2O$ (10): Yield: 71.51%, yellow, m.p.: > 300 ºC, *m.w.*: 592.97, Anal. calcd. (found) (%) for $C_{22}H_{21}N_7O_5S_2Zn$: C, 44.56 (44.50); H, 3.57 (3.50); N, 16.54 (16.60); IR (KBr, ν_{max}, cm^{-1}): 3500, 3186 (OH)/(N-H), 3041 (CH)aryl, 1620 (C=O) amide(I), 1620 (C=N), 1537 amide (II), 1199 (C-O), 2090 (M-NCS, terminal), 468 δ(NCS), 532 (M-O), 468 (M-N); ^{13}C NMR (400 MHz, solid, δ, ppm): 167.60 (CONH), 162.62 (C=N, azomethine), 156.27, 148.65, 134.58, 110.45 (pyridine ring), 154.12 (C-O), 118.65-134.58 (aromatic ring); molar conductance (DMSO): 12.81 Ω^{-1} cm^2 mol^{-1}; μ_{eff} (B.M.): diamagnetic.

$[Mn(HL_3)(NCS)(H_2O)_2]NCS\cdot H_2O$ (11): Yield: 70.31%, yellow, m.p.: 203 ºC, *m.w.*: 562.49, Anal. calcd. (found) % for $C_{19}H_{21}N_7O_6S_2Mn$: C, 40.57 (40.61); H, 3.76 (3.80); N, 17.43 (17.38); IR (KBr, ν_{max}, cm^{-1}): 3376, 3147 (OH)/(N-H), 1637 (C=O) amide(I), 1597 (C=O, chromone), 1537 (C=N), 2057 (M-NCS, terminal), 484 δ(NCS), 508 (M-O), 462 (M-N); UV-Vis (λ_{max}) (DMSO): 19,267 cm^{-1} [$^6A_{1g}$ (S) $\rightarrow$ $^4T_{1g}$ (G)] octahedral; ESI-MS (*m/z* value for M^+): 561; molar conductance (DMSO): 54 Ω^{-1} cm^2 mol^{-1}; μ_{eff} (B.M.): 5.71.

$[Co(L_3)(NCS)]\cdot 2H_2O$ (12): Yield: 67.31%, brown, m.p.: > 300 ºC, *m.w.*: 489.38, Anal. calcd. (found) % for $C_{18}H_{18}N_6O_5SCo$: C, 44.18 (44.06); H, 3.71 (3.72); N, 17.17 (17.20); IR (KBr, ν_{max}, cm^{-1}): 3224 (OH)/(N-H), 1618 (C=O, chromone), 1618 (C=N-N=C), 2075 (M-NCS, terminal), 615 (M-O), 440 (M-N); UV-Vis (λ_{max}) (DMSO): 21,929 cm^{-1} ($A_{1g} \rightarrow B_{1g}$) square planar; ESI-MS (*m/z* value for M^+): 491; molar conductance (DMSO): 28 Ω^{-1} cm^2 mol^{-1}; μ_{eff} (B.M.): 2.8.

$[Ni(HL_3)(NCS)]NCS\cdot 3H_2O$ (13): Yield: 69.51%, green, m.p.: 260 ºC, *m.w.*: 566.25, Anal. calcd. (found) % for $C_{19}H_{21}N_7O_6S_2Ni$: C, 40.30 (40.25); H, 3.74 (3.75); N, 17.32 (17.28); IR (KBr, ν_{max}, cm^{-1}): 3387, 3212 (OH)/(N-H), 1645 (C=O) amide (I), 1610 (C=O, chromone), 1533 (C=N), 2105 (M-NCS, terminal), 480 ∂(NCS), 506 (M-O), 448 (M-N); UV-Vis (λ_{max}) (DMSO): 13,333 cm^{-1} [$^3T_1(F) \rightarrow {}^3T_1(P)$ (ν_3)] distorted tetrahedral; ESI-MS (*m/z* value for M^+): 565, 566; molar conductance (DMSO): 45 Ω^{-1} cm^2 mol^{-1}; μ_{eff} (B.M.): 2.8.

$[Cu(HL_3)(Cl)(H_2O)_2]Cl\cdot 3H_2O$ (14): Yield: 72.21%, green, m.p.: 210 ºC, *m.w.*: 561.87, Anal. calcd. (found) % for $C_{17}H_{25}N_5O_8Cl_2Cu$: C, 36.34 (36.40); H, 4.49 (4.42); N, 12.46 (12.52); IR (KBr, ν_{max}, cm^{-1}): 3367 (OH)/(N-H), 1638 (C=O) amide (I), 1613 (C=O, chromone), 1568 (C=N), 506 (M-O), 487 (M-N); UV-Vis (λ_{max}) (DMSO): 13,642 cm^{-1} ($^2B_{1g} \rightarrow {}^2A_{1g}$) distorted octahedral; ESI-MS (*m/z* value for M^+): 565; molar conductance (DMSO): 39 Ω^{-1} cm^2 mol^{-1}; μ_{eff} (B.M): 1.9.

$[Zn(HL_3)(NCS)_2(H_2O)]$ (15): Yield: 72.21%, yellow, m.p.: 219 ºC, *m.w.*: 536.90, Anal. calcd. (found) % for $C_{19}H_{17}N_7O_4S_2Zn$: C, 42.50 (42.45); H, 3.19 (3.12); N, 18.26 (18.34); IR (KBr, ν_{max}, cm^{-1}): 3440, 3229 (OH)/(N-H), 1669 (C=O) amide (I), 1632 (C=O, chromone), 1522 (C=N), 2072 (M-NCS, terminal), 480 δ(NCS), 525 (M-O), 416 (M-N); ^{13}C NMR (400 MHz, solid, δ, ppm): 176.98, 173.27 (C=O) (amide and *exo*), 168.19 (azomethine carbon), 154.12 (C-O, chromone), 113.87, 116.119, 122.27, 127.54 (chromone moiety carbons), 158.90, 149.23-136.92, 118.95, 109.76 (pyridine ring), 22.04 (CH_3); molar conductance (DMSO): 11 Ω^{-1} cm^2 mol^{-1}; μ_{eff} (B.M.): diamagnetic.

$[Co(L_4)(NCS)_3]\cdot 2H_2O$ (16): Yield: 69.61%, brown, m.p.: 220 ºC, *m.w.*: 606.55, Anal. calcd. (found) % for $C_{20}H_{19}N_8O_5S_3Co$: C, 39.60 (39.54); H, 3.16 (3.12); N, 18.47 (18.40); IR (KBr, ν_{max}, cm^{-1}): 3512, 3213 (OH)/(N-H), 1672 (C=O) amide (I), 1626 (C=O, *exo*), 1579 (C=N), 1548 amide (II), 2085 (M-NCS, terminal), 509 (M-O), 443 (M-N); ^1H NMR (400 MHz, DMSO-

d_6, δ, ppm): 8.02 (s, 1H, CONH), 6.96-7.66 (m, 7H, aromatic ring), 4.80 (s, 1H, OH, enol), 3.22 (s, 2H, NH_2), 2.09 (s, 3H, CH_3); UV-Vis (λ_{max}) (DMSO): 21,834 cm^{-1} ($^1A_{1g} \rightarrow {}^1T_{1g}$) octahedral; ESI-MS (*m/z* value for M^+): 610; molar conductance (DMSO): 3.48 Ω^{-1} cm^2 mol^{-1}; μ_{eff} (B.M.): diamagnetic.

$[Ni(L_4)(NCS)_2(H_2O)]\cdot 3H_2O$ (17): Yield: 68.91%, orange, m.p.: 230 ºC, *m.w.*: 584.26, Anal. calcd. (found) % for $C_{19}H_{23}N_7O_7S_2Ni$: C, 39.06 (39.12); H, 3.97 (3.88); N, 16.78 (16.74); IR (KBr, ν_{max}, cm^{-1}): 3230 (OH)/(N-H), 1651 (C=O) amide (I), 1622 (C=O, *exo*), 1573 (C=N), 1539 amide (II), 2100 (M-NCS, terminal), 678 (M-O), 534 (M-N); UV-Vis (λ_{max}) (DMSO): 12,043, 15,151, 24,330 cm^{-1} [$^3A_{2g}(F) \rightarrow {}^3T_{2g}(F)$ (ν_1), $^3A_{2g}(F) \rightarrow {}^3T_{1g}(F)$ (ν_2), $^3A_{2g}(F) \rightarrow {}^3T_{1g}(P)$ (ν_3)] octahedral; ESI-MS (*m/z* value for M^+): 584.2; molar conductance (DMSO): 21.64 Ω^{-1} cm^2 mol^{-1}; μ_{eff} (B.M.): 2.9.

$[Cu(L_4)(NCS)_2(H_2O)]\cdot H_2O$ (18): Yield: 69.21%, green, m.p.: 240 ºC, *m.w.*: 553.08, Anal. calcd. (found) % for $C_{19}H_{19}N_7O_5S_2Cu$: C, 41.26 (41.15); H, 3.46 (3.42); N, 17.73 (17.67); IR (KBr, ν_{max}, cm^{-1}): 3502, 3176 (OH)/(N-H), 1687 (C=O) amide (I), 1631 (C=O, *exo*), 1566 (C=N), 1541 amide (II), 2092 (M-NCS, terminal), 426 (M-O), 403 (M-N); UV-Vis (λ_{max}) (DMSO): 14,792 cm^{-1} ($^2B_{1g} \rightarrow {}^2A_{1g}$) distorted octahedral; ESI-MS (*m/z* value for M^+): 550.2; molar conductance (DMSO): 12.86 Ω^{-1} cm^2 mol^{-1}; μ_{eff} (B.M.): 1.9.

DNA binding studies: To understand the DNA binding mode as well as affinity of the newly synthesized ligands and their eighteen complexes to CT-DNA, three methods namely electronic absorption, cyclic voltammetry and viscosity measurements have been studied.

RESULTS AND DISCUSSION

Eighteen metal complexes were synthesized using the four different Schiff base ligands [**Schemes I-IV**]. Solubility of Schiff base ligand **HL_3** is less as compared to **L_1**, **HL_2** and **L_4** in DMSO. Complexes **1-4**, **6**, **8**, **9**, **11**, **13**, **14**, **16**, **17** and **18** are soluble in DMF and DMSO whereas, complexes **5**, **10** and **15** are less soluble in cold DMSO. Complexes **7** and **12** are soluble in most organic solvents. Complexes **2**, **3**, **5**, **8**, **9**, **10**, **11**, **13**, **15**, **17** and **18** have been found to have 1:1:2 while complexes **4** and **12** are 1:2:2 and 1:1:1 (metal:primary ligand:secondary ligand) ratios, respectively. Complexes **1**, **7** and **14** have 1:1 and **6** has 1:2 (metal: primary ligand) ratio while complex **16** has 1:1:3 (metal: primary ligand: secondary ligand) ratio. From the conductance data, it is clear that complexes **2**, **8**, **11**, **13** and **14** have 1:1 electrolyte type and others are non-electrolyte [36]. All the complexes are stable in air. For Cu(II) complex **4**, low μ_{eff} value (1.37 B.M.) at room temperature from the theoretical value for one unpaired electron system may be attributed to anti-ferromagnetic interaction between Cu(II) metal ions in solid form. Hence, there might be a close relationship between the ν(C-N) band at 2117 cm^{-1} of the thiocyanate ligand and low μ_{eff} value of this complex. That is, bonding mode of the thiocyanate ligand might be bridging. Further, room temperature μ_{eff} value of 4.13 B.M. for complex **6** in solid form was found rather deviate from spin free Mn(II) high spin system (5.92 B.M.) as compared to other two complexes **1** (5.21 B.M.) and **11** (5.71 B.M.). Such a lower value may come from an extensive exchange interaction between Mn(II) centres in a solid state [37].

EPR spectral feature of this complex in powder form at LNT is seen very broad which supports the above fact (Fig. 1e). As well, complexes **1** and **11** have correspondingly a broad sextet (Fig. 1d) and a broad isotropic signal (Fig. 1f) in powder form at LNT. Even though the complexes have different spectral features in solid form, these complexes have a hyperfine sextet in DMSO at LNT. Also, a hyperfine splitting is easily seen for a high spin Mn^{2+} (I = 5/2) system when nuclear spin interacts with the electron spin of the same atom. Thus, geometries of complexes **1**, **6** and **11** have been assigned as octahedral around the metal centres with the EPR spectral features [Fig. 1a for (**1**); Fig. 1b for (**6**) and Fig. 1c for (**11**)].

Infrared study: IR spectrum of L_1 has shown absorption bands at 3211, 3138 and 3036 cm^{-1} due to ν(N-H) and ν(C-H) stretching vibrations of amine, amide and aromatic ring respectively [38]. Spectra of **L_1** also showed bands at 1689, 1643, 1627 and 1535 cm^{-1}, indicating the presence of amide (I) (C=O), chromone moiety (C=O), azomethine bond (C=N) and amide (II) respectively [39,40]. Again, the spectrum of **HL_2** exhibited bands at 3572, 3232 and 3059 cm^{-1}, which may be assigned to ν(O-H), ν(N-H) and ν(C-H) stretching vibrations of phenoxo, amine, amide and aromatic ring, respectively. In addition, amide (I) (C=O), azomethine bond (C=N) and amide (II) absorption bands of **HL_2** have appeared at 1635, 1606 and 1537 cm^{-1} respectively. Phenoxo ν(C-O) stretching band was appeared at 1201 cm^{-1} [41] and seen to remain unchanged in their positions for complexes **6**, **8**-**10**. Therefore, participation of phenoxo oxygen in bonding after deprotonating in these complexes were excluded while in complex **7**, it might be taken as stretching vibration of the functional group ν(O-H) was observed differently at 3431 cm^{-1} as well as an increase in stretching band of ν(C-O) group at 1247 cm^{-1} when compared to the values of these two functional groups of the Schiff base ligand, **HL_2** [42]. The appearance of the band at 3431 cm^{-1} may be responsible for another (O-H) or (N-H) group present in the ligand.

In **HL_3**, vibrational bands appeared at 3444, 3339 and 3206 cm^{-1} could be assigned for ν(O-H)/ν(N-H) stretching vibrations of lattice water [43], amine and amide groups respectively. Other bands at 1685, 1649 and 1618 cm^{-1} have been assigned to amide (I) (C=O), chromone moiety (C=O) and azomethine bond (C=N), respectively. The spectrum of **L_4** has prominent bands at 3491, 3315 and 3217 cm^{-1} which could be assigned for ν(O-H)/ν(N-H) stretching vibrations of lattice water/enol, amine and amide groups, respectively. Besides, bands at 1693, 1643, 1591 and 1537 cm^{-1} have been assigned to amide (I) (C=O), indane moiety (C=O), azomethine bond (C=N) and amide (II), respectively.

Amide ν(C=O) stretching bands are almost the same in complexes **4**-**5** while in complexes **1**-**3**, **6**-**11, 13**-**18** decreases in the range (6-48) cm^{-1} indicating the participation of oxygen atom in bonding. Shifting of exo-cyclic ν(C=O) stretching bands by about 4-31, 17-52 and 12-21 cm^{-1} of chromone and indane moieties in the complexes of **L_1**, **HL_3** and **L_4** indicate the participation of oxygen atom in metal coordination respec-

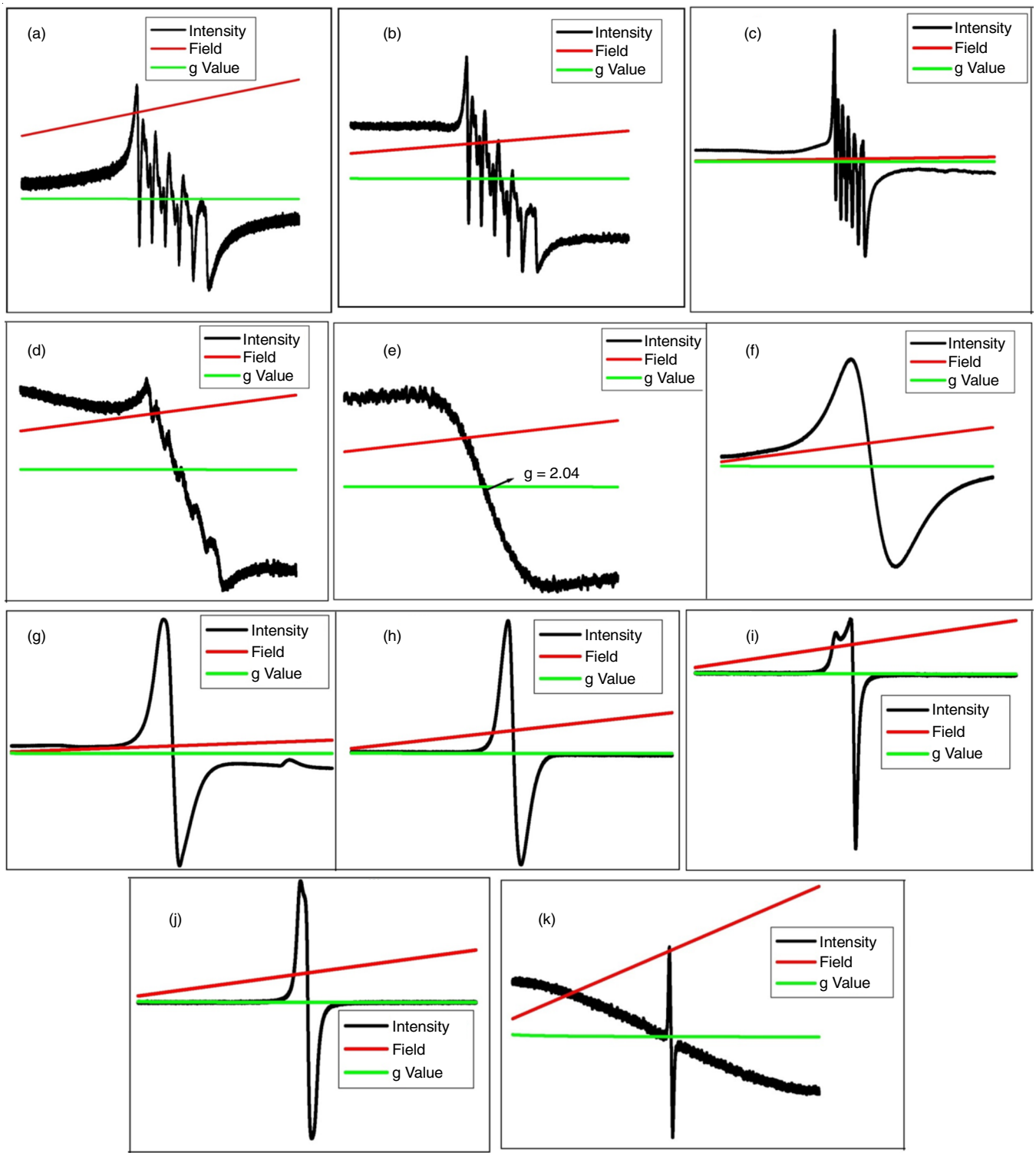

Fig. 1. (a) EPR spectra of complex **1**, (b) for complex **6**, and (c) for complex **11** in DMSO at LNT; (d) for complex **1**, (e) for complex **6**, (f) for complex **11**, (g) for complex **4**, (h) for complex **9**, (i) for complex **14**, (j) for complex **18** and (k) for complex **12** in powder form at LNT

tively. Moreover, bonding between metal and azomethine nitrogen atoms was confirmed by the observable shifting of ν(C=N) stretching bands in either positive or negative direction [44].

In complex **1**, two new bands (1629 and 1344 cm^{-1}) and their peak separation [$\Delta = \nu_{as}(COO^-) - \nu_s(COO^-)$] equal to 285 cm^{-1} could be attributed to asymmetric and symmetric stretching vibrations of the monodentate acetate group [45,46]. In complexes **2-5**, **8**, **10-13**, **15-18**, ν(C-N) stretching frequencies of thiocyanate appeared in the range of 2057-2117 cm^{-1} indicating the formation of metal-thiocyanato bonds. In complex **4,** observation of ν(C-N) absorption band at 2117 cm^{-1} has indicated

the bonding mode of thiocyanate group as bridging while in other complexes, it remains as terminal because the ν(C-N) absorption bands are less than the 2100 cm^{-1} [47]. An asymmetric stretching band of the azide group was observed at 2063 cm^{-1} for complex **9** which falls at terminal absorption vibration [48]. The of bands at 1444 and 1305 cm^{-1} in complex **7** have been assigned to ν_4 and ν_1 frequencies of the coordinated nitrate group of monodentate type. The separation between these two highest bands is found to be one of the criteria to determine the binding mode of the nitrate group which is less than 130 cm^{-1} but in present case, it is found as 139 cm^{-1} [49]. In complex **12,** a strong new azine band (C=N–N=C) at 1618 cm^{-1} was observed indicating the absence of amide I (C=O) stretching band and subsequent coordination in enol form after deprotonation [40,50-52]. Additional bands observed in the range of 3599-3224 cm^{-1} in metal complexes **1-3**, **8**, **10-18** may be assigned to ν(O-H) stretching of lattice or coordinated water molecules [53]. Metal-nitrogen and metal-oxygen bonding also proved by the new bands which appeared in the regions 534-403 cm^{-1} and 678-426 cm^{-1}, respectively.

Electronic study: Generally, high-spin manganese(II) complexes show rare *d-d* transitions due to spin Laporte forbidden in octahedral complexes. However, complexes **1**, **6** and **11** have shoulder type of absorption bands at 30,120, 22,935 and 19267 cm^{-1} which tentatively assign to $^6A_{1g}(S) \rightarrow {}^4E_g(D)$, $^6A_{1g}(S) \rightarrow {}^4T_{2g}(G)$ and $^6A_{1g}(S) \rightarrow {}^4T_{1g}(G)$ forbidden transitions of an octahedral geometry respectively [54]. The spectrum of Co(II) complex **2** has an absorption band at 13,333 cm^{-1}, attributable to $^4A_2(F) \rightarrow {}^4T_1(P)$ (ν_3) transition of a tetrahedral geometry [55,56] whereas, complexes (**7** and **12**) have correspondingly a strong absorption band at 22,624 and 21,929 cm^{-1} which were found to be correlated with a low-spin Co(II) square planar geometry [57,58]. Co(III) complex **16** has a strong absorption band at 21,834 cm^{-1}, assignable to $^1A_{1g} \rightarrow {}^1T_{1g}$ transition of a low spin octahedral geometry [59,60]. Ni(II) complexes **3** and **17** have three absorption bands in each at (13,106, 16,207, 26,737) and (12,043, 15,151, 24,330) cm^{-1}, attributed to $^3A_{2g}(F) \rightarrow {}^3T_{2g}(F)$ (ν_1), $^3A_{2g}(F) \rightarrow {}^3T_{1g}(F)$ (ν_2) and $^3A_{2g}(F) \rightarrow {}^3T_{1g}(P)$ (ν_3) transitions of an octahedral geometry and ν_2/ν_1 values in these complexes were found to be lowered than the reported value [61]. Whereas, Ni(II) complexes **8** and **13** have absorption bands at 13,262 and 13,333 cm^{-1}, assigned to $^3T_1(F) \rightarrow {}^3T_1(P)$ (ν_3) transition of a distorted tetrahedral geometry [62]. In Cu(II) complexes (**4**, **14** and **18**), broad asymmetric bands at 14,534, 13,642 and 14,792 cm^{-1} were observed which may assign to $^2B_{1g} \rightarrow {}^2A_{1g}$ transition of a distorted octahedral geometry. However, Cu(II) complex **9** has an absorption band at 15,772 cm^{-1}, suggestive of a square planar geometry [63,64].

^{1}H NMR study: The solution (DMSO-d_6) ^{1}H NMR spectrum of ligand, $\mathbf{L_1}$ has signals at δ (10.80) (s, 1H), δ(8.93) (s, 1H), δ(8.28) (s, 1H), δ(7.59-7.89) (m, 4H), δ(3.36) (s, 2H) and δ(2.48) (s,3H) ppm, which may be assigned to the protons of amide, (N-H), azomethine, aromatic ring, amine and methyl groups respectively. And, for $\mathbf{HL_2}$, signals at δ(8.35) (s, 1H), δ(8.40) (s, 2H), δ(6.86-8.18) (m, 11H), δ(8.61) (s, 1H) and δ(8.74) (s, 1H) ppm were assigned for (NH), azomethine, aromatic ring, amide (CONH) and phenoxo (Ar-OH) protons respectively. Also, the spectrum of $\mathbf{L_4}$ has signals at δ(8.66) (s, 1H), δ(6.83-8.07) (m, 8H), δ(3.14) (s, 2H), δ(2.48) (s, 3H) ppm which may be assigned to the protons of amide, aromatic ring, amine and methyl groups respectively. Whereas, signals of Co(III) complex of $\mathbf{L_4}$ (**16**) has appeared at δ(8.02) (s, 1H), δ(6.96-7.66) (m, 7H), δ(4.80) (s, 1H), δ(3.22) (s, 2H), δ(2.09) (s, 3H) ppm which have assigned correspondingly to the protons of amide, aromatic ring, enol, amine and methyl groups respectively. Thus, it has concluded, in complex **16,** one of the two exo C=O behaves in enol form in contrast to $\mathbf{L_4}$. Again, the signal of (N-H) is found to be absent in both ligand as well as complex.

^{13}C NMR study: In the solid-state ^{13}C NMR spectrum of $\mathbf{HL_3}$, signals at δ(176.00-174.44), δ(153.53), δ(133.70), δ(115.14-127.25), δ(158.22, 142.10, 139.07, 136.53, 107.52), δ(22.72) ppm may be assigned to C=O (amide and exo), C-O, C=N, chromone moiety carbons, pyridine ring and CH_3 group respectively. Complex **5** has shown signals at δ(21.65), δ(112.79-146.79), δ(153.63), δ(166.33) and δ(176) ppm, which have assigned correspondingly for CH_3, chromone moiety, C-O, C=N and C=O of exo and amide. In complex **10**, signals at δ(167.60), δ(162.62), δ(156.27, 148.65, 134.58, 110.45), δ(154.12) and δ(118.65-134.58) ppm have assigned relatively for CONH, C=N, pyridine ring, C-O and aromatic ring. Complex **15**, has shown signals at δ(176.98-173.27), δ(168.19), δ(154.12), δ(113.87, 116.119, 122.27, 127.54), δ(158.90, 149.23-136.92, 118.95, 109.76) and δ(22.04) ppm, which have assigned correspondingly for (C=O) (amide and exo), azomethine carbon, C-O, chromone moiety carbons, pyridine ring and CH_3.

EPR study: Manganese complexes **1, 6** and **11** have a well-resolved sextet signal in the solution spectra (DMSO) at LNT with g_{iso} values of 2.01, 2.01 and 2.04, respectively [Figs. 1(a-c)]. These values are found to be near the free-electron spin value of 2.00, indicating the +2 oxidation state of metal ions which were getting supplement by the observed hyperfine coupling constants (A_{iso}) that lies within the range of 78-83 G. It was also seen in complexes **1** and **6**, forbidden transitions corresponding to $\Delta m_I = \pm 1$ are more prominent than complex **11** between each of two main hyperfine lines due to the mixing of nuclear hyperfine levels with zero field splitting factors [65]. At LNT, the powder form of complex **1** has a broad sextet signal with $g_{iso} = 2.01$ while a broad isotropic signal of the complexes **6** and **11** was observed with g_{iso} values of 2.04 and 1.88 respectively [Figs. 1(d-f)]. Broadness of the spectra may be due to the dipolar interaction and enhanced spin-lattice relaxation [66]. Besides, complex **11** in DMSO at RT has a hyperfine sextet signal with $g_{iso} = 2.04$.

Again, spectra of Cu(II) complexes **4**, **9** and **18** were of isotropic type in powder form at LNT with g_{iso} values of 2.02, 2.01 and 2.09, respectively while Cu(II) complex **14** has an anisotropic signal with $g_{\parallel} = 2.18$ and $g_{\perp} = 2.06$. Value of $g_{\parallel}$ (< 2.3) and trend in g values ($g_{\parallel} > g_{\perp} > 2.0023$) has suggested the metal-ligand bonding of covalent type and presence of unpaired electron in $d_{x^2-y^2}$ orbital [67]. Further, G value was calculated using the equation, $G = (g_{\parallel}-2.002)/(g_{\perp}-2.002)$ and found to be 3.1, suggesting a strong field ligand [Figs. 1(g-j)]. For Co(II)

complex **12**, EPR signal was isotropic with g_{iso} value of 1.98 in powder form at both RT and LNT (Fig. 1k).

Powder-XRD study: Diffraction patterns of four ligands (**L_1**, **HL_2**, **HL_3** and **L_4**) and nine complexes (**2**, **3**, **4**, **5**, **9**, **11**, **13**, **14** and **15**) are shown in Fig. 2(a-m). The average crystallite sizes (d_{xrd}) were calculated using the Debye-Scherrer's equation, $d_{xrd} = 0.9\ \lambda/\beta \cos\theta$. In this equation, β, θ and λ represent the full width at half maximum of the dominant peak, Bragg's reflection angle and wavelength of CuK_α radiation (1.5406 Å) respectively [68]. Crystallite sizes are present as 12.9 (**L_1**), 11 (**HL_2**), 9.43 (**HL_3**), 14.5 (**L_4**), 32.37 (**2**), 28.35 (**3**), 25.0 (**4**), 31.66 (**5**), 19.83 (**9**), 24.7 (**11**), 27.56 (**13**), 26.75 (**14**) and 16.5 nm (**15**) and found within the nano-range except for ligand (**HL_3**). Unit cell parameters were derived using the program P-index. A monoclinic system for complexes **2** and **14** has been found whereas a triclinic system for the ligands and complexes **3**, **4**, **5**, **9**, **11**, **13** and **15**. Unit cell parameters are given as follows: a = 32.8111, b = 12.6159, c = 9.8937 Å, α = 82.674, β = 101.023, γ = 103.861º, V = 758.73 Å^3(**L_1**); a = 7.3538, b = 6.3321, c = 9.2828 Å, α = 72.747, β = 99.832, γ = 100.153º, V = 403.09 Å^3(**HL_2**); a = 8.51, b = 6.9006, c = 5.2179 Å, α = 76.462, β = 106.209, γ = 125.895º, V = 237.38 Å^3(**HL_3**); a = 9.6068, b = 8.4587, c = 10.4886 Å, α = 83.442, β = 113.079, γ = 126.651º, V = 620.74 Å^3(**L_4**); a = 8.0052, b = 7.2226, c = 13.8212 Å, β = 148.276º, V = 2153.50 Å^3(**2**); a = 6.2230, b = 4.7092, c = 12.8609 Å, α = 115.047, β = 134.143, γ = 80.150º, V = 240.54 Å^3(**3**); a = 4.2611, b = 4.1551, c = 8.4466 Å, α = 103.260, β = 92.306, γ = 101.932º, V = 141.81 Å^3(**4**); a = 11.4975, b = 9.3451, c = 7.3162 Å, α = 85.785, β = 90.688, γ = 46.909º, V = 570.40 Å^3(**5**); a = 7.8383, b = 6.6486, c = 5.0464 Å, α = 62.692, β = 96.709, γ = 103.362º, V = 227.33 Å^3 (**9**); a = 4.7183, b = 3.9851, c = 7.8146 Å, α = 113.424, β = 125.285, γ = 78.015º, V = 110.01 Å^3 (**11**); a = 4.4210, b = 8.3125, c = 6.8908 Å, α = 106.988, β = 93.619, γ = 100.406º, V = 236.39 Å^3 (**13**); a = 10.3977, b = 7.0238, c = 10.1644 Å, β = 147.409º, V = 399.85 Å^3 (**14**); a = 5.9315, b = 11.5217, c = 15.8435 Å, α = 138.849, β = 136.907, γ = 62.144º, V = 478.50 Å^3 (**15**).

TG-DTA study: Thermal study of the complexes (**1-18**) was performed within the temperature range of 30-900 °C in a nitrogen atmosphere. Complex **1** (Fig. 3a) showed three decomposition steps in the temperature ranges of 129-156, 167-253 and 254-744 ºC, due to the loss of six lattice water molecules, one coordinated water molecule and one ligand molecule (**L_1**) respectively. For complex **2** (Fig. 3b), two decomposition steps were noticed in the temperature ranges of 134-146 and 225-846 °C due to the loss of one lattice water molecule and two thiocyanate ions plus one ligand molecule (**L_1**). Two decomposition steps of complex **3** (Fig. 3c) were found in the temperature ranges of 140-162 and 163-694 ºC due to the loss of one lattice plus one coordinated water molecule and two thiocyanate ions plus one ligand molecule (**L_1**). In complex **4** (Fig. 3d), the first and second decomposition steps were seen in the temperature ranges of 219-484 and 485-844 ºC due to the expulsion of two thiocyanate ions plus one ligand molecule (**L_1**) and another ligand molecule (**L_1**). In complex **5** (Fig. 3e), gradual decomposition in one step was found in the temperature range of 200-844 ºC due to the loss of two thiocyanate ions and one ligand molecule (**L_1**). Two decomposition steps for the complex **6** (Fig. 3f) were seen in the temperature ranges of 221-418 and 419-898 ºC due to the loss of two chloride ions plus one ligand molecule (**HL_2**) and another ligand molecule (**HL_2**). In complex **7** (Fig. 3g), gradual decomposition was seen in the temperature range of 230-690 ºC due to the loss of one coordinated nitrate ion and one ligand molecule (**HL_2**). For complex **8** (Fig. 3h), decomposition starts at 130 ºC and continues up to 844 ºC due

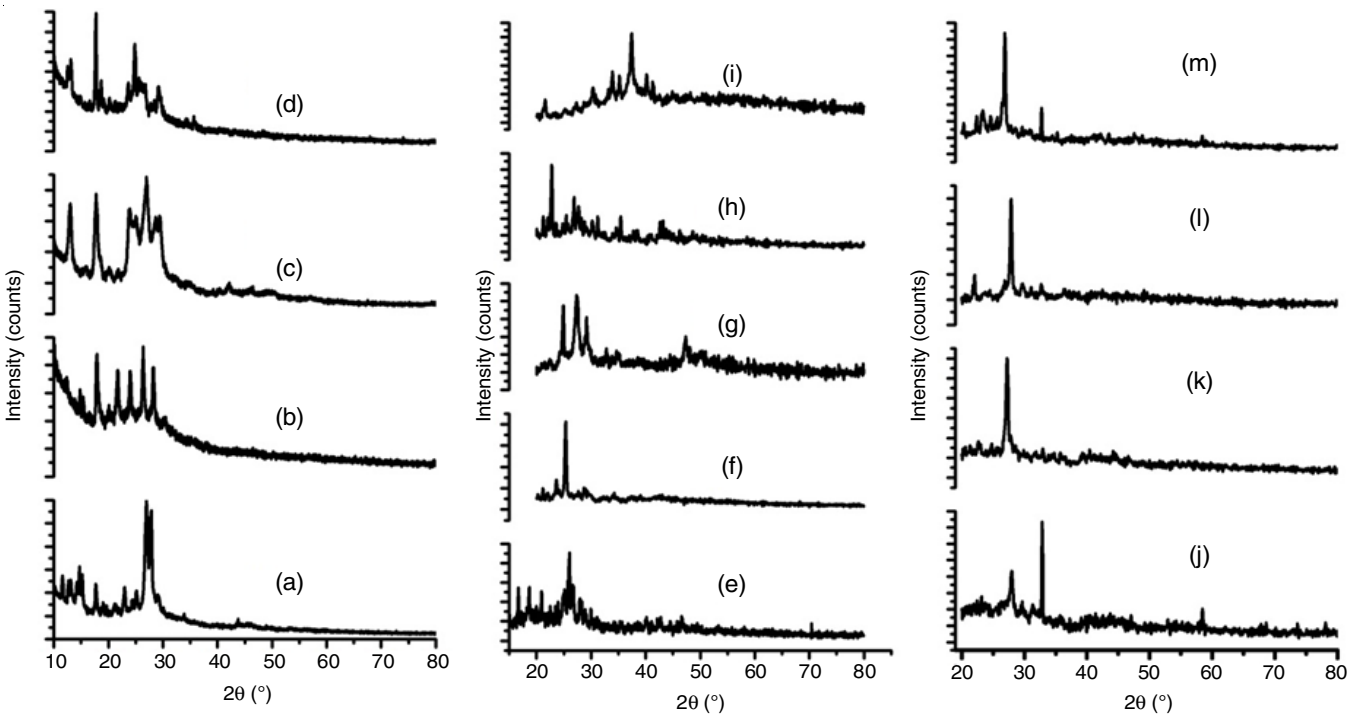

Fig. 2(a-m). PXRD diffraction patterns of the four ligands (a,b,c and d) and their metal complexes (**2-5, 9**, **11**, **13**, **14**, and **15**)

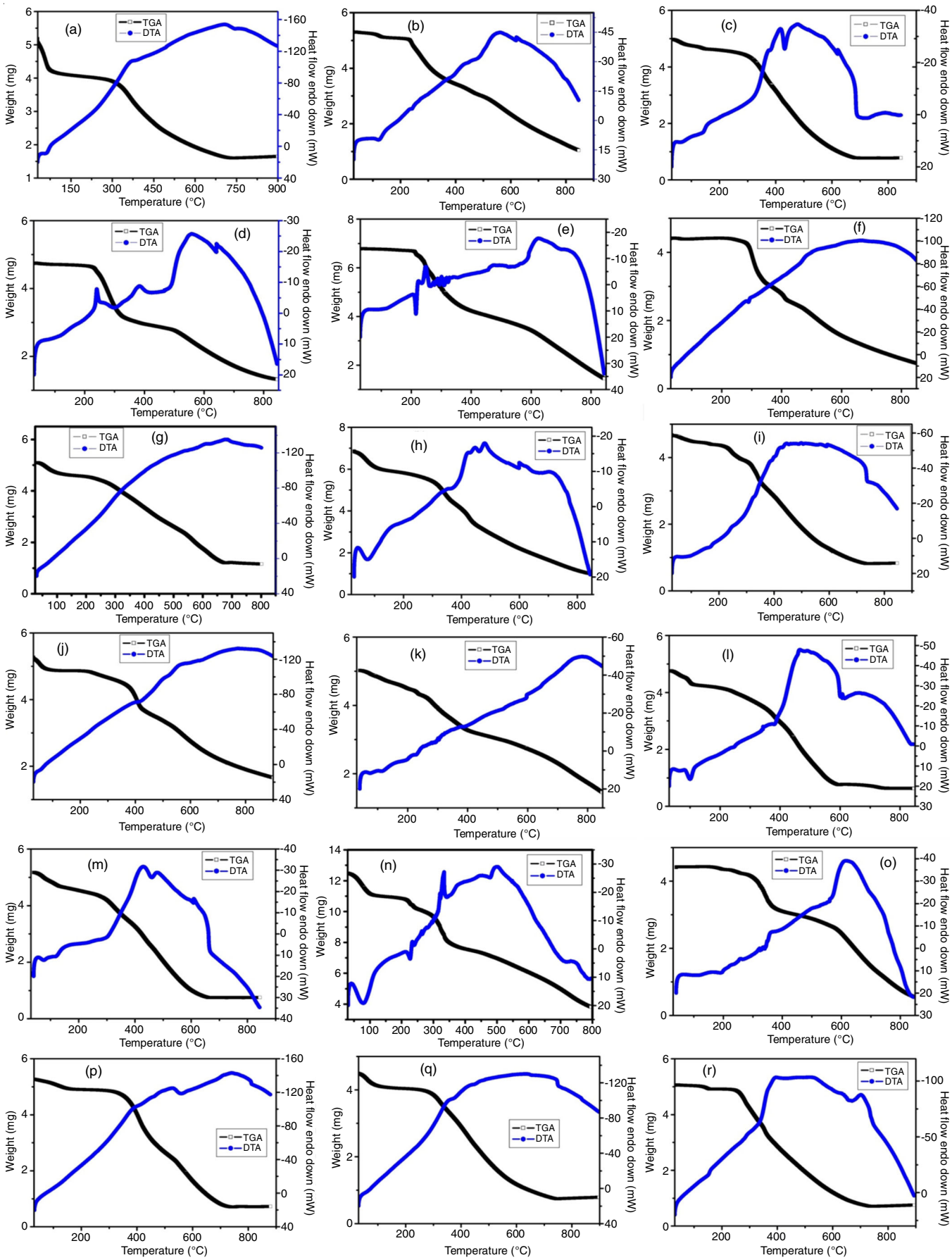

Fig. 3(a-r).TGA-DTA spectra of the metal complexes (**1-18**)

to the loss of two water molecules (one lattice and one coordinated), two thiocyanate ions and one ligand molecule (HL_2). In complex **9** (Fig. 3i), gradual decomposition started at 139 ºC and continued up to 750 ºC due to the loss of two azide ions and one ligand molecule (HL_2). In complex **10** (Fig. 3j), three decomposition steps were seen in the temperature ranges of 130-100, 182-431 and 432-899 ºC due to the loss of two lattice water molecules, two thiocyanate ions and one ligand molecule (HL_2). In complex **11** (Fig. 3k), gradual decomposition started at 140 ºC and continued up to 847 ºC due to the loss of three water molecules (one lattice and two coordinate), two thiocyanate ions and one ligand molecule (HL_3). In complex **12** (Fig. 3l), one decomposition step was seen in the temperature range of 141- 600 ºC due to the loss of two lattice water molecules, one thiocyanate ion and one ligand molecule (HL_3). In complex **13** (Fig. 3m), gradual decomposition started at 140 ºC and continued up to 661 ºC due to the loss of three lattice water molecules, two thiocyanate ions and one ligand molecule (HL_3). Decomposition in complex **14** (Fig. 3n) was seen in the temperature range of 131-795 ºC due to the loss of five water molecules (three lattices and two coordinate), two chloride ions and one ligand molecule (HL_3). In complex **15** (Fig. 3o), decomposition started at 142 ºC and continued upto 845 ºC due to the expulsion of one coordinated water molecule, two thiocyanate ions and one ligand molecule (HL_3). Decomposition of complex **16** (Fig. 3p) was seen in the temperature range of 132-750 ºC due to the loss of two lattice water molecules, three thiocyanate ions and one ligand molecule (L_4). In complex **17** (Fig. 3q), decomposition started at 130 °C and continues upto 751 °C due to the loss of four water molecules (three lattices and one coordinate), two thiocyanate ions and one ligand molecule (L_4). The first and second decomposition steps of complex **18** (Fig. 3r) were seen in the temperature ranges of 134-166 and 229-759 ºC due to the loss of one lattice water molecule and one coordinated water molecule, two thiocyanate ions plus one ligand molecule (L_4).

DNA binding studies

Electronic titration method: Preparation of buffer (5 mM *tris*-HCl and 50 mM NaCl) (pH = 7.2), as well as DNA stock solution in buffer, checking of DNA purity, determination of DNA stock concentration and titration procedure are all similar as described in previous work [69]. Also, ligands and metal complexes were dissolved in DMSO to prepare the respective solutions. All the ligands and their complexes have shown a decrease in intensity (hypochromic effect) with the addition of CT-DNA in an augmented mode of concentration in the intra-ligand bands at 281 (L_1, Fig. 4a), 346 (HL_2, Fig. 5), 351 (HL_3, Fig. 4b), 388 [L_4, Fig. 4c), 330 (**1**, Fig. 4d), 334 (**2**, Fig. 4e), 327 (**3**, Fig. 4f), 344 (**4**, Fig. 4g), 318 (**5**, Fig. 4h), 354 (**6**, Fig. 4i), 424 (**7**, Fig. 4j), 411 (**8**, Fig. 4k), 413 (**9**, Fig. 4l), 391 (**10**, Fig. 4m), 343 (**11**, Fig. 4n), 438 (**12**, Fig. 4o), 380 (**13**, Fig. 4p), 433 (**14**, Fig. 4q), 362 (**15**, Fig. 4r), 420 (**16**, Fig. 4s), 382 (**17**, Fig. t) and 403 nm (**18**, Fig. 4u). A red shift of about 2 nm of the ligand (HL_3), 8.5 nm for the ligand (L_4), 7 nm for the complex **1** and 3 nm for the complex **8** were observed whereas a blue shift of about 2.5 nm for the ligand (L_1), 1.5 nm for the ligand (HL_2), 3 nm for the complex **6**, 2 nm for the complex **9**, 10 nm for the complex **10**, 17 nm for the complex **15** and 3 nm for the complex **17** were observed. Additionally, an isosbestic point for the complexes **2** (279 nm), **3** (287 nm), **4** (292 nm), **5** (274 nm), **6** (285 nm), **7** (287 nm), **8** (285 nm), **9** (282 nm), **10** (277 nm), **11** (287 nm), **12** (286 nm), **13** (285 nm), **14** (262 nm), **15** (290 nm) and **18** (288 nm) were seen. Therefore, it is a sign of retaining equilibrium between the two species that is, metal complex is free from and metal complex bound to DNA in solution. Such a spectral change is a key indicator of the interaction of the ligands and their complexes with the CT-DNA. Usually, a drop in the spectral intensity

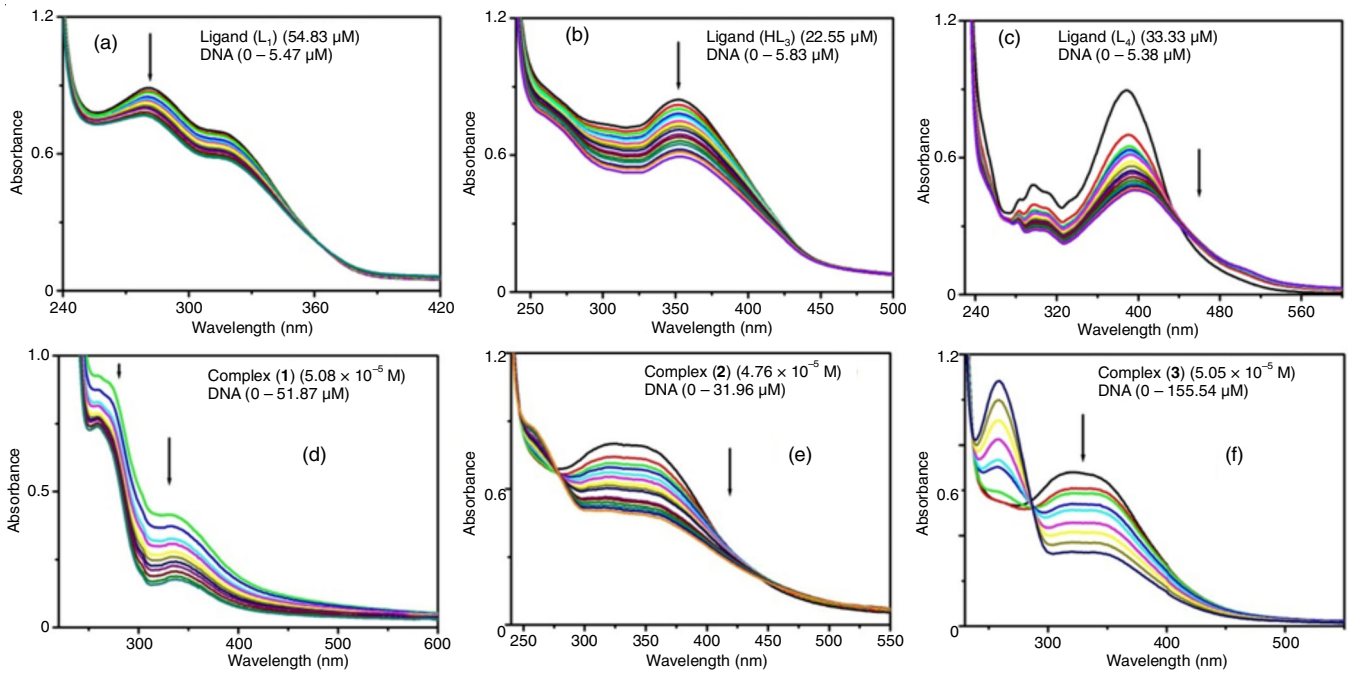

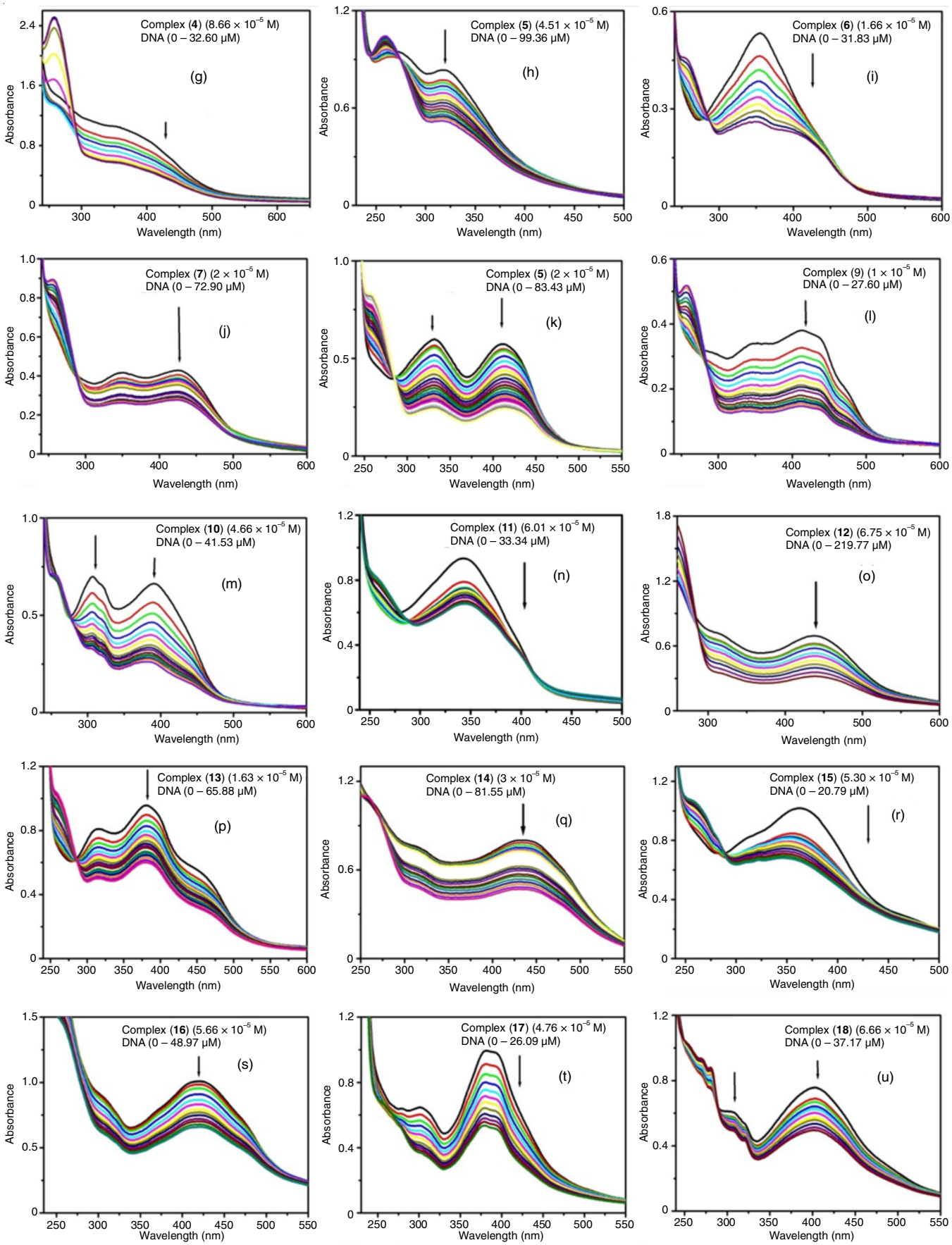

Fig. 4(a-u). Effect on absorption spectra of the ligands ($\mathbf{L_1}$, $\mathbf{HL_3}$ and $\mathbf{L_4}$) and thier metal complexes (**1-18**) at fixed concentrations in Tris-HCl buffer (pH = 7.2) with the increase in the DNA concentration, respectively

was observed for DNA intercalators with or without the shift in the absorption maxima with the addition of DNA [70]. Besides, a decrease in absorption intensity may be involved with the partial intercalative or groove binding mode [71]. Thus, an absorption titration method was unable to give a full confirmation about the DNA binding mode of small molecules. The binding affinity of the complexes could be assessed through the intrinsic binding constant (K_b) using eqn. 1:

$$\frac{[DNA]}{(\varepsilon_a - \varepsilon_f)} = \frac{[DNA]}{(\varepsilon_b - \varepsilon_f)} + [K_b(\varepsilon_b - \varepsilon_f)]^{-1} \quad (1)$$

where, [DNA], ε_a, ε_f and ε_b represents the DNA concentration in base pairs, apparent, free and bound metal complexes extinction coefficients respectively. K_b is the ratio of the slope to the intercept obtained by plotting [DNA]/(ε_a-ε_f) against [DNA] [72]. The K_b value of the ligands and complexes were obtained as 2.64×10^5 (**L_1**), 4.48×10^4 (**HL_2**), 3.78×10^4 (**HL_3**), 4.55×10^5 (**L_4**), 1.41×10^4 (**1**), 2.3×10^4 (**2**), 1.20×10^4 (**3**), 4.9×10^4 (**4**), 6.43×10^3 (**5**), 6.2×10^4 (**6**), 1.27×10^4 (**7**), 7.94×10^4 (**8**), 7.07×10^4 (**9**), 7.05×10^3 (**10**), 1.11×10^5 (**11**), 1.47×10^4 (**12**), 2.2×10^4 (**13**), 1.78×10^4 (**14**), 5.99×10^4 (**15**), 7.6×10^3 (**16**), 3.23×10^4 (**17**) and 7.8×10^3 M^{-1} (**18**). It was noticed that the K_b values of the ligands and complexes are lowered than the value of the classical intercalator, EB (1.4×10^6 M^{-1}) [73]. The binding affinity of the Mn(II) complexes (**1**, **6** and **11**) falls within the range of $7.97 \times 10^3 - 1.35 \times 10^5$ M^{-1} [74-76] and for cobalt (II)/(III) complexes (**2**, **7**, **12** and **16**) are found to be less than the DNA intercalators [77]. Also, K_b values of the Ni(II) complexes (**3**, **8**, **13** and **17**) are comparable with those of moderate as well as the intercalative binders having a magnitude of the order (10^4 M^{-1}) [78,79]. Cu(II) complexes (**4**, **9**, **14** and **18**) were found to have K_b values greater than 1.6×10^3 M^{-1} [80] or comparable with 4×10^4 M^{-1} of the DNA intercalators [81]. Again, K_b values of Zn(II) complexes (**5**, **10** and **15**) are comparable to the partially intercalating Zn(II) complex having a magnitude of order (10^3-10^4 M^{-1}) [82]. After comparison, the trend in K_b values of the first, second, third, fourth ligand and their respective complexes were found in the order **L_1** > **4** > **2** > **1** > **3** > **5**, **8** > **9** > **6** > **HL_2** > **7** > **10**, **11** > **15** > **HL_3** > **13** > **14** > **12** and **L_4** > **17** > **18** > **16**, respectively. The effect of CT-DNA in the absorption intensity of **HL_2** has shown in Fig. 5.

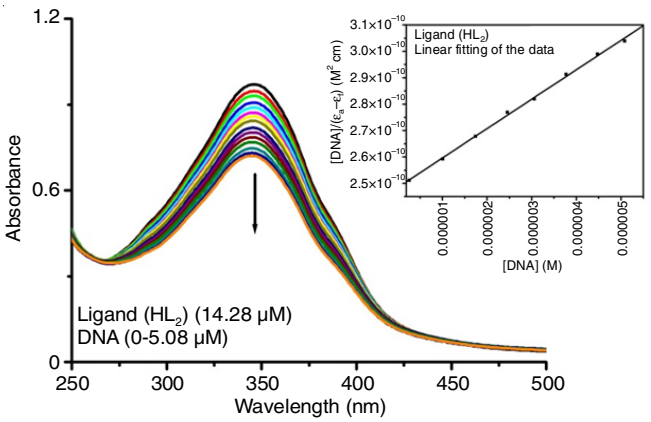

Fig. 5. Absorption spectra of ligand (**HL_2**) in Tris-HCl buffer (pH = 7.2) that shows the effect of DNA interaction in terms of its intensity's decreases. Inset: Corresponding plot of [DNA]/ε_a-ε_f *vs.* [DNA]

Cyclic voltammetry method: DNA binding study of the ligands (**HL_3** and **L_4**) and complexes (**1**-**18**) was also performed in a single compartmental cell having a three-electrode system. One is a glassy carbon working electrode while the other two are Pt-wire auxiliary electrode and an Ag/$AgNO_3$ reference electrode. The electrochemical evaluations were performed within +0.8 V to -2 V at a 0.01 V/s scan rate in *tris*-buffer (pH = 7.2) at room temperature. TBAB (0.1M, in double-distilled water) was used as a supporting electrolyte. The method is simply to monitor the change in the electrochemical behaviour of the ligands and their metal complexes at a constant concentration in the absence and presence of varying CT-DNA concentrations. In complex **1** (Fig. 6d), the first cathodic and anodic peaks move in positive potentials while the second cathodic peak has vanished with the addition of CT-DNA. For complex **2** (Fig. 6e), two cathodic peaks move to little negative potentials while anodic peak almost at the potential value with the addition of CT-DNA. In complex **3** (Fig. 6f), one cathodic and one anodic peak is seen in the presence of CT-DNA, moves correspondingly to negative and positive potential. In complex **4** (Fig. 6g), cathodic peaks move in positive potentials whereas the anodic peak is almost at the same position in the presence of CT-DNA. In complex **5** (Fig. 6h), cathodic and anodic peaks move in correspondingly negative and positive potentials in the presence of CT-DNA. In complex **6** (Fig. 6i), it is seen those two cathodic peaks almost at the same positions while anodic peak moves in positive potential with the addition of CT-DNA. For complex **7** (Fig. 6j), second cathodic peak has disappeared while first cathodic and anodic peak move in positive potentials in the presence of CT-DNA. In complex **8** (Fig. 6k), it was found that cathodic peaks moved in positive potentials while anodic peak moved in negative potential with the addition of CT-DNA. In the presence of CT-DNA, complex **9** (Fig. 6l) had shown one cathodic peak (-0.642 V) that lacked in the absence of CT-DNA whereas the anodic peak moves in positive potential. For complex **10** (Fig. 6m), it was found to move in positive potentials for the cathodic waves whereas, for the anodic wave, it was in the negative potential in the presence of CT-DNA. In addition of CT-DNA to the ligand (**HL_3**) (Fig. 7), first cathodic peak moved in negative potential whereas second cathodic peak and two anodic peaks moved in positive potentials. For complex **11** (Fig. 6n), first cathodic and anodic peaks move in positive potentials while second cathodic peak move in negative potential in the presence of CT-DNA. Complex **12** (Fig. 6o) has one cathodic peak that moved in positive potential in the presence of CT-DNA. For complex **13** (Fig. 6p), in the addition of CT-DNA, both cathodic and anodic peaks moved in positive potentials. In complex **14** (Fig. 6q), cathodic peak moved in positive potential while anodic peak was almost at the same potential in the presence of CT-DNA. First cathodic and second anodic waves of the complex **15** (Fig. 6r) moved in negative potentials while second cathodic and first anodic peaks moved in positive potentials in the presence of CT-DNA. For ligand **L_4** (Fig. 6c), first cathodic peak moved in negative potential whereas second cathodic and anodic waves were appeared to shift in positive potentials in the presence of CT-DNA. For complex **16** (Fig. 6s), first

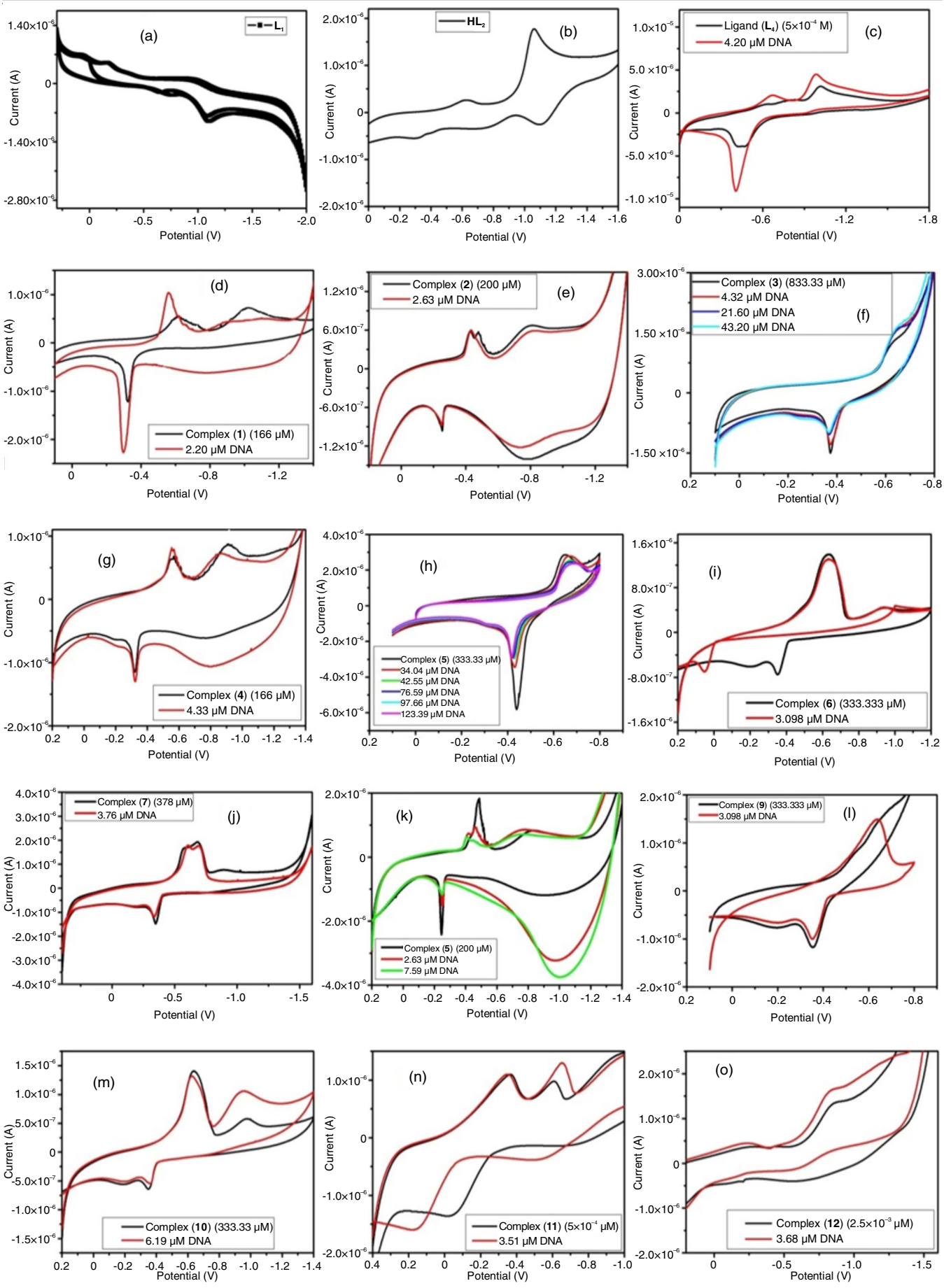
(a)
L1
(b)
HL2
(c)
Ligand (L4) (5×10-4 M)
4.20 μM DNA
(d)
Complex (1) (166 μM)
2.20 μM DNA
(e)
Complex (2) (200 μM)
2.63 μM DNA
(f)
Complex (3) (833.33 μM)
4.32 μM DNA
21.60 μM DNA
43.20 μM DNA
(g)
Complex (4) (166 μM)
4.33 μM DNA
(h)
Complex (5) (333.33 μM)
34.04 μM DNA
42.55 μM DNA
76.59 μM DNA
97.66 μM DNA
123.39 μM DNA
(i)
Complex (6) (333.333 μM)
3.098 μM DNA
(j)
Complex (7) (378 μM)
3.76 μM DNA
(k)
Complex (5) (200 μM)
2.63 μM DNA
7.59 μM DNA
(l)
Complex (9) (333.333 μM)
3.098 μM DNA
(m)
Complex (10) (333.33 μM)
6.19 μM DNA
(n)
Complex (11) (5×10-4 μM)
3.51 μM DNA
(o)
Complex (12) (2.5×10-3 μM)
3.68 μM DNA
Current (A)
Potential (V)

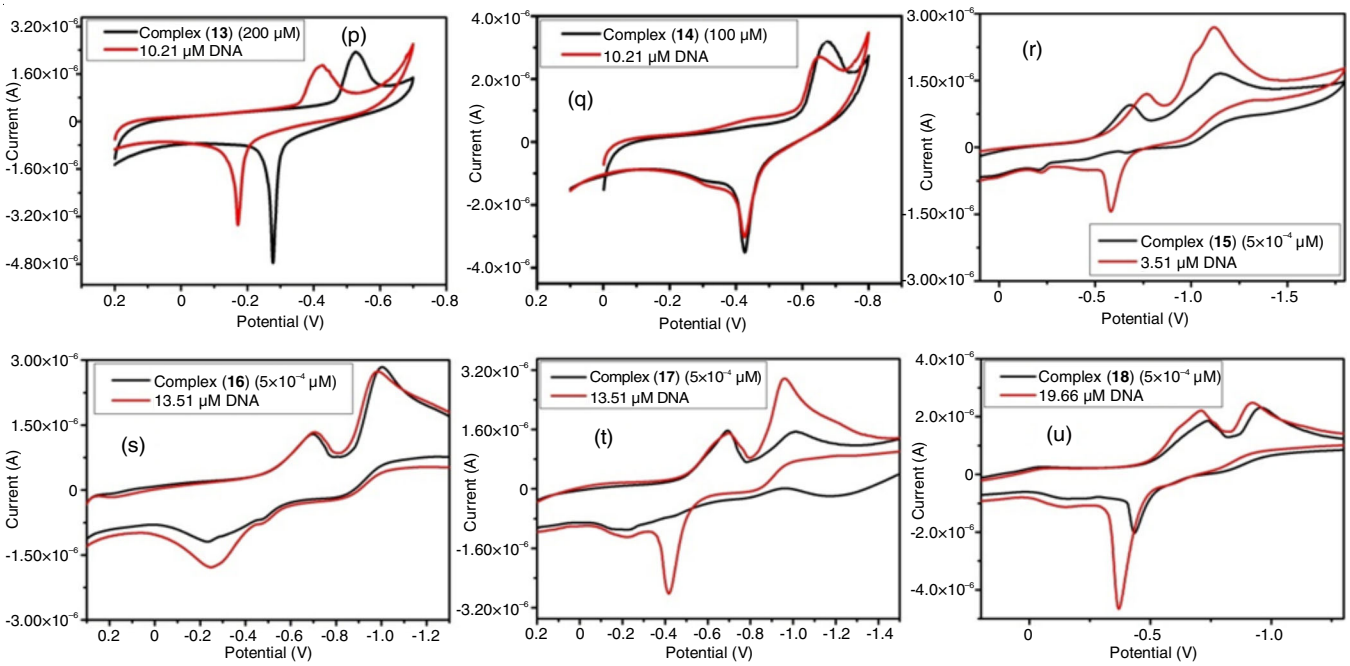

Fig. 6(a-u). Cyclic voltammograms of the ligands ($\mathbf{L_1}$, $\mathbf{HL_2}$ and $\mathbf{L_4}$) and their metal complexes (**1-18**) in Tris-HCl buffer (pH = 7.2) in the absence and presence of CT-DNA, respectively

cathodic and anodic waves moved in negative potentials while second cathodic peak moved in positive potential in the presence of CT-DNA. In the addition of CT-DNA, first cathodic and anodic peaks of the complex **17** (Fig. 6t) moved in negative potentials while second cathodic peak moved in positive potential. For complex **18** (Fig. 6u), all the three (two cathodic and one anodic) peaks were seen to move in positive potentials in the addition of CT-DNA. It has been found that ΔE_p values are greater than 59 mV for the two ligands and complexes in both free and bound cases thereby redox processes are irreversible. In complexes **1**, **2**, **4**, **6**, **7**, **8**, **10**, **11**, **15**, **16**, **17** and **18**, appearance of second cathodic peaks may be responsible for ligand centered electrode process while first cathodic peaks of all complexes may be responsible of metal centered redox processes [M(II)/M(I)]. First redox couples (-0.703 and -0.182 V; -0.647 and -0.430 V) of ligands ($\mathbf{HL_3}$ and $\mathbf{L_4}$) might be related to the conversion process of functional group C=O to C–OH and its reverse reaction [83]. Whereas second redox couples (-1.095 V and -0.495 V; -1.018 V) of these two ligands may be conversion process of functional group N=N-CH to C=N and its reverse reaction [84]. A change in peak current intensity was observed with the addition of CT-DNA in all of the two ligands and complexes. In Table-1, experimental data of the ligands and complexes are given. Cyclic voltammogram of the ligand ($\mathbf{HL_3}$) with or without CT-DNA is given in Fig. 7 whereas CV spectra for the remaining three ligands ($\mathbf{L_1}$, $\mathbf{HL_2}$ and $\mathbf{L_4}$) and complexes (**1**-**18**) are also obtained (Fig. 6a-u). From the CV data, it is seen that the formal potential E^o or voltammetric $E_{1/2}$ for the complexes (**1**, **4**, **6**, **7**, **8**, **13**, **14 and 18**) shift in positive potentials while in ligands ($\mathbf{HL_3}$ and $\mathbf{L_4}$) and complexes **2**, **3**, **5**, **10**, **11**, **15**, **16** and **17**, shifted in negative potentials insignificantly in the presence of CT-DNA. Complexes **9** and **12** have a positive shift in potential value even though

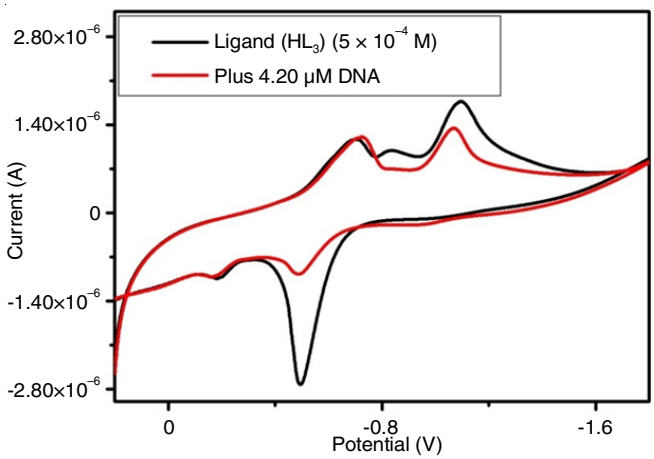

Fig. 7. Cyclic voltammogram of ligand ($\mathbf{HL_3}$) in Tris-HCl buffer (pH = 7.2) that shows the effect of CT-DNA when it is present in the solution

cathodic and anodic peaks are not able to see in both free as well as bound conditions. Generally, a positive shift in formal potential values was concluded for an intercalative mode of binding with CT-DNA whereas a shift in a negative value for the formal potential as an electrostatic mode of binding [85]. Thus, complexes **1**, **4**, **6**, **7**, **8**, **13**, **14** and **18** may bind primarily through an intercalative mode whereas ligands ($\mathbf{HL_3}$ and $\mathbf{L_4}$) and complexes **2**, **3**, **5**, **10**, **11** and **15**-**17** may bind with the CT-DNA in a partial intercalation or groove binding mode as the negative shift in formal potential values are insignificant. Besides, complexes **9** and **12** may bind in an intercalative way.

Viscosity measurement: To deduce an exact binding mode, viscosity measurement at a fixed concentration of the CT-DNA with the variable concentration of the ligands and their metal complexes was performed. An intercalative binding mode of small molecules indeed involves DNA viscosity to

TABLE-1
CV RESULTS OF THE LIGANDS AND THEIR METAL COMPLEXES WITH OR WITHOUT CT-DNA

Complex/ Ligand	E_{pc} (V)		E_{pa} (V)		ΔE_p (V)		$E_{1/2}$ (V)	
	Free	Bound	Free	Bound	Free	Bound	Free	Bound
L_1	-0.770 (c_1)	*	-0.166	*	0.604	*	- 0.468	*
	-1.109(c_2)	*	-	-	-	-	-	-
1	-0.614(c_1)	-0.560(c_1)	-0.323	-0.296	0.291	0.264	-0.468	-0.428
	-1.022 (c_2)	-	-	-	-	-	-	-
2	-0.427(c_1)	-0.433(c_1)	-0.253	-0.250	0.174	0.183	-0.340	-0.341
	-0.814 (c_2)	-0.829(c_2)	-	-	-	-	-	-
3	-0.631	-0.642	-0.374	-0.369	0.257	0.273	-0.502	-0.505
4	-0.566(c_1)	-0.553(c_1)	-0.322	-0.324	0.244	0.229	-0.444	-0.438
	-0.910(c_2)	-0.868(c_2)	-	-	-	-	-	-
5	-0.651	-0.662	-0.439	-0.431	0.212	0.231	-0.545	-0.546
HL_2	-0.626 (c_1)	*	-0.292	*	0.334	*	-0.459	*
	-1.061 (c_2)	*	-	-	-	-	-	-
6	-0.634(c_1)	-0.633(c_1)	-0.352	-0.348	0.282	0.285	-0.493	-0.490
	-0.945(c_2)	-0.942(c_2)	-	-	-	-	-	-
7	-0.684(c_1)	-0.609(c_1)	-0.349	-0.338	0.335	0.271	-0.516	-0.473
	-0.898(c_2)	-	-	-	-	-	-	-
8	-0.487(c_1)	-0.459(c_1)	-0.248	-0.254	0.239	0.205	-0.367	-0.356
	-0.835(c_2)	-0.790(c_2)	-	-	-	-	-	-
9	-	-0.642	-0.354	-0.352	-	0.290	-	-0.497
10	-0.638(c_1)	-0.625(c_1)	-0.349	-0.363	0.289	0.262	-0.493	-0.494
	-0.975(c_2)	-0.958(c_2)	-	-	-	-	-	-
HL_3	-0.703(c_1)	-0.725(c_1)	-0.182(a_2)	-0.163(a_2)	0.521	0.562	-0.443	-0.444
	-1.095(c_2)	-1.069(c_2)	-0.495(a_1)	-0.489(a_1)	0.6	0.58	-0.795	-0.779
11	-0.366(c_1)	-0.349(c_1)	-0.048	0.150	0.318	0.499	- 0.207	-0.099
	-0.607(c_2)	-0.653(c_2)	-	-	-	-	-	-
12	-0.859	-0.841	-	-	-	-	-	-
13	-0.527	-0.426	-0.277	-0.170	0.250	0. 256	-0.402	-0.298
14	-0.674	-0.652	-0.427	-0.425	0.247	0.227	-0.550	-0.538
15	-0.684(c_1)	-0.768(c_1)	-0.206(a_2)	-0.215(a_2)	0.478	0.553	-0.445	-0.491
	-1.157(c_2)	-1.120(c_2)	-0.662(a_1)	-0.581(a_1)	0.495	0.539	-0.909	-0.850
L_4	- 0.647(c_1)	-0.672(c_1)	-0.430	-0.407	0.217	0.265	-0.538	-0.539
	-1.018(c_2)	-0.986(c_2)	-	-	-	-	-	-
16	-0.696(c_1)	-0.706(c_1)	-0.231	-0.248	0.465	0.458	-0.463	-0.477
	-1.004(c_2)	-0.983(c_2)	-	-	-	-	-	-
17	-0.694(c_1)	-0.700(c_1)	-0.220	-0.418	0.474	0.282	-0.457	-0.559
	-1.011(c_2)	-0.961(c_2)	-	-	-	-	-	-
18	-0.739(c_1)	-0.710(c_1)	-0.434	-0.369	0.305	0.341	-0.586	-0.539
	-0.957(c_2)	-0.922(c_2)	-	-	-	-	-	-

*Implies L_1 and HL_2 are not studied their binding interaction with CT-DNA; c_1 and c_2 represent the first and second cathodic peaks; a_1 and a_2 are used to imply first and second anodic peaks; $E_{1/2} = ½ (E_{pa} + E_{pc})$ and $\Delta E_p = E_{pa} - E_{pc}$.

increase, an electrostatic binding mode to decrease its viscosity and a groove binding mode accounts for a little or no effect on its viscosity [86]. A graphical representation of relative viscosity $(\eta/\eta_o)^{1/3}$ *vs.* [compound]/[DNA] of the ligands (**L_1-L_4**) and complexes (**1**, **4**, **6-9**, **11-15**, **17** and **18**) in Fig. 8 while for complexes (**2**, **3**, **5**, **10** and **16**) in Fig. 9 is presented. Thus, complexes **1**, **4**, **6-9**, **12-14** and **18** may bind with CT-DNA in an intercalative mode as the viscosity of DNA increase in a moderate way whereas ligands (**L_1**, **HL_2**, **HL_3** and **L_4**) and complexes (**2-3**, **5**, **10-11** and **15-17**) may bind in a partial intercalative mode as the viscosity of DNA increase to a lesser extent as compared to others.

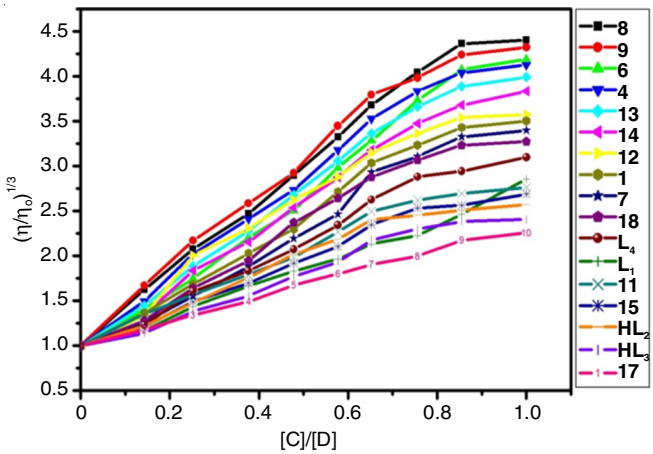

Fig. 8. Graphical representation on relative specific viscosity variation of CT-DNA solution (2.0×10^{-5} M) in presence of the ligands (**L_1-L_4**) and complexes (**1**, **4**, **6-9, 11-15, 17-18**) (0 – 2.0×10^{-5} M) in Tris-HCl buffer (pH = 7.2) at 25 °Cs

Conclusion

Eighteen metal complexes of four different Schiff base ligands, (1*E*)-1-((6-methyl-4-oxo-4*H*-chromen-3-yl)methylene)-carbohydrazide (**L_1**), 6-[2 (salicylidene)hydrazinyl]-*N*′-(salicylidene)nicotinohydrazide (**HL_2**), 6-hydrazinyl-*N*′-(6-

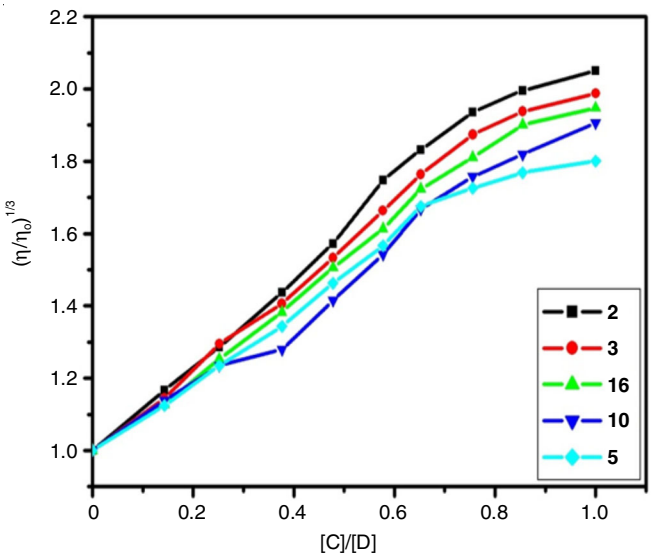

Fig. 9. Graphical representation on relative specific viscosity variation of CT-DNA solution (2.0×10^{-5} M) in presence of the complexes (**2**, **3**, **5**, **10**, and **16**) (0 – 2.0×10^{-5} M) in Tris-HCl buffer (pH = 7.2) at 25 °C

methyl-4-oxo-4*H*-chromen-3-yl-methylene)nicotinohydrazide (**HL_3**) and (*E*)-6-hydrazinyl-*N*′-(1-(2,3-dihydro-1,3-dioxo-1*H*-inden-2-yl)-ethylidene)pyridine-3-carbohydrazide (**L_4**) were synthesized and characterized. In the absence of single crystals, plausible geometries were proposed of all the complexes using the various spectroscopic methods (elemental analyses, IR, UV-Vis, NMR, MS, TGA/DTA, EPR and PXRD). Schiff bases *viz*. **L_1** and **HL_2** acting either tridentate (ONO) or bidentate (ON) donor whereas **HL_3** and **L_4** acting only tridentate (ONO) donor to develop different coordination environment around the metal ions. In complex **12**, **HL_3** participates in enol form but it is in keto form on the other complexes. Data obtained from room temperature magnetic moment, electronic absorption and molar conductance are consistent with the complex structures except for complexes **4** and **6**. The low magnetic moment of these two complexes in solid state may arise from antiferromagnetic interaction present in the magnetically concentrated system. EPR study confirms +2 oxidation states of three manganese complexes (**1**, **6** and **11**) with high-spin octahedral configuration and a paramagnetic nature of the Cu(II) (**4**, **9**, **14**, **18**) and Co(II) (**12**) complexes. Cumulative results of the CT-DNA binding study dictates the primary binding mode of the complexes (**1**, **4**, **6**-**9**, **12**-**14** and **18**) is intercalative whereas ligands (**L_1**, **HL_2**, **HL_3** and **L_4**) and complexes (**2**, **3**, **5**, **10**, **11**, **15**, **16** and **17**) may a partial intercalative mode. Binding affinity trend for the intercalators follows the order: **8 > 9 > 6 > 4 > 13 > 14 > 12 > 1 > 7 > 18** while for the partial intercalators are in the order **L_4 > L_1 > 11 > 15 > HL_2 > HL_3 > 17 > 2 > 3 > 16 > 10 > 5**.

ACKNOWLEDGEMENTS

The authors are pleased to acknowledge the SAIF, IIT Bombay, Mumbai, North-Eastern Hill University, Shillong, I.I.Sc. Bangalore and CDRI, Lucknow for providing EPR, ^{1}H NMR, ^{13}C NMR and MS data. Thanks are also due to UGC, New Delhi, India for financial assistance.

CONFLICT OF INTEREST

The authors declare that there is no conflict of interests regarding the publication of this article.

REFERENCES

1. K. Sudeepa, N. Narsimha, B. Aparna, S. Sreekanth, A.V. Aparna, M. Ravi, J. Mohmed and C.H.S. Devi, *J. Chem. Sci.*, **130**, 52 (2018); https://doi.org/10.1007/s12039-018-1437-0
2. E.E. Sengül, T. Göktürk, C.G. Topkaya and R. Gup, *J. Chil. Chem. Soc.*, **65**, 4754 (2020).
3. S.A. Aly and S.K. Fathalla, *Arab. J. Chem.*, **13**, 3735 (2020); https://doi.org/10.1016/j.arabjc.2019.12.003
4. H.A. El-Wahab, *Prog. Org. Coat.*, **89**, 106 (2015); https://doi.org/10.1016/j.porgcoat.2015.08.001
5. M.M.E. Shakdofa, M.H. Shtaiwi, N. Morsy and T.M.A. Abdel-rassel, *Main Group Chem.*, **13**, 187 (2014); https://doi.org/10.3233/MGC-140133
6. S.M. Annigeri, M.P. Sathisha and V.K. Revankar, *J. Coord. Chem.*, **61**, 4011 (2008); https://doi.org/10.1080/00958970802199956
7. D. Dragancea, S. Shova, É.A. Enyedy, M. Breza, P. Rapta, L.M. Carrella, E. Rentschler, A. Dobrov and V.B. Arion, *Polyhedron*, **80**, 180 (2014); https://doi.org/10.1016/j.poly.2014.03.039
8. S.S. Tandon, M.-C. Dul, J.L. Lee, L.N. Dawe, M.U. Anwar and L.K. Thompson, *Dalton Trans.*, **40**, 3466 (2011); https://doi.org/10.1039/c0dt01487g
9. C. Bustos, O. Burckhardt, R. Schrebler, D. Carrillo, A.M. Arif, A.H. Cowley and C.M. Nunn, *Inorg. Chem.*, **29**, 3996 (1990); https://doi.org/10.1021/ic00345a017
10. M. Sutradhar, T.R. Barman and E. Rentschler, *Inorg. Chem. Commun.*, **39**, 140 (2014); https://doi.org/10.1016/j.inoche.2013.11.018
11. E.R. krishna, P.M. Redd, M. Sarangapani, G. Hanmanthu, B. Geeta, K.S. Rani and V. Ravinder, *Spectrochim. Acta A Mol. Biomol. Spectrosc.*, **97**, 189 (2012); https://doi.org/10.1016/j.saa.2012.05.073
12. D.P. Singh, V. Grover, P. Rathi and K. Jain, *Arab. J. Chem.*, **10**, S1795 (2017); https://doi.org/10.1016/j.arabjc.2013.07.004
13. Y. Harinath, D. Harikishore Kumar Reddy, B. Naresh Kumar, C. Apparao and K. Seshaiah, *Spectrochim. Acta A Mol. Biomol. Spectrosc.*, **101**, 264 (2013); https://doi.org/10.1016/j.saa.2012.09.085
14. A.K. Sharma and S. Chandra, *Spectrochim. Acta A Mol. Biomol. Spectrosc.*, **103**, 96 (2013); https://doi.org/10.1016/j.saa.2012.11.012
15. G.B. Pethe, A.R. Yaul and A.S. Aswar, *Bull. Chem. Soc. Ethiop.*, **29**, 387 (2015); https://doi.org/10.4314/bcse.v29i3.6
16. O.S. Bushuyev, F.A. Arguelles, P. Brown, B.L. Weeks and L.J. Hope-Weeks, *Eur. J. Inorg. Chem.*, **2011**, 4622 (2011); https://doi.org/10.1002/ejic.201100465
17. M.A. Kamyabi, F. Soleymani-Bonoti, R. Bikas, H. Hosseini-Monfared, N. Arshadi, M. Siczek and T. Lis, *Phys. Chem. Chem. Phys.*, **17**, 32161 (2015); https://doi.org/10.1039/C5CP04695E
18. G.B. Pethe, N.J. Suryawanshi and A.S. Aswar, *J. Basic Sci. Appl. Res.*, **1**, 1 (2015).
19. S. Chandra, Deepshikha and A. Sarkar, *Arab. J. Chem.*, **10**, S1306 (2017); https://doi.org/10.1016/j.arabjc.2013.03.015
20. S. Chandra, Deepshikha and A. Sarkar, *Spectrochim. Acta A Mol. Biomol. Spectrosc.*, **107**, 271 (2013); https://doi.org/10.1016/j.saa.2013.01.055
21. O. Babaiah, C. Kesavarao, T. Sreenivasulureddy and V. Krishnareddy, *Talanta*, **43**, 551 (1996); https://doi.org/10.1016/0039-9140(95)01766-6
22. L. Fan, T. Li, B. Wang, Z. Yang and C. Liu, *Spectrochim. Acta A Mol. Biomol. Spectrosc.*, **118**, 760 (2014); https://doi.org/10.1016/j.saa.2013.09.062

23. K.S. Abou-Melha, *Spectrochim. Acta A Mol. Biomol. Spectrosc.*, **70**, 162 (2008); https://doi.org/10.1016/j.saa.2007.07.023
24. G. Klopman, D. Fercu and J. Jacob, *Chem. Phys.*, **204**, 181 (1996); https://doi.org/10.1016/0301-0104(95)00415-7
25. A. Moradi, L. Navidpour, M. Amini, H. Sadeghian, H. Shadnia, O. Firouzi, R. Miri, S.E.S. Ebrahimi, M. Abdollahi, M.H. Zahmatkesh and A. Shafiee, *Arch. Pharm. Chem. Life Sci.*, **343**, 509 (2010); https://doi.org/10.1002/ardp.200900294
26. L. Changzheng, W. Jigui, W. Liufang, R. Min, J. Naiyong and G. Jie, *J. Inorg. Biochem.*, **73**, 195 (1999); https://doi.org/10.1016/S0162-0134(99)00005-7
27. D. Sharma, H.D. Revanasiddappa and B. Jayalakshmi, *Egypt. J. Basic Appl. Sci.*, **7**, 323 (2020); https://doi.org/10.1080/2314808X.2020.1758890
28. Y. Li, Z.Y. Yang and M.F. Wang, *J. Fluoresc.*, **20**, 891 (2010); https://doi.org/10.1007/s10895-010-0635-z
29. N. Raman, A. Sakthivel and N. Pravin, *Spectrochim. Acta A Mol. Biomol. Spectrosc.*, **125**, 404 (2014); https://doi.org/10.1016/j.saa.2014.01.108
30. S. Janardan, P. Suman, G. Swapna, A. Amrita, R. Priya, R. Siva, K. Vijayakrishna and A. Sivaramakrishna, *Appl. Biochem. Biotechnol.*, **173**, 596 (2014); https://doi.org/10.1007/s12010-014-0868-4
31. P. Jayaseelan, S. Prasad, S. Vedanayaki and R. Rajavel, *Arab. J. Chem.*, **9**, S668 (2016); https://doi.org/10.1016/j.arabjc.2011.07.029
32. N. Vamsikrishna, M.P. Kumar, G. Ramesh, N. Ganji, S. Daravath and Shivaraj, *J. Chem. Sci.*, **129**, 609 (2017); https://doi.org/10.1007/s12039-017-1273-7
33. O. U-Wang R.K.B. Singh, W.B. Devi, U.I. Singh, R.K.B. Devi, O.B. Devi, R. Shahani and T. Swu, *Inorg. Nano-Met. Chem.*, **49**, 363 (2019); https://doi.org/10.1080/24701556.2019.1661457
34. W.B. Devi, R.K.B. Singh, J.P. Jasinski and J.A. Golen, *Inorg. Chem. Commun.*, **21**, 163 (2012); https://doi.org/10.1016/j.inoche.2012.05.006
35. R.K.B. Devi, S.P. Devi, R.K.B. Singh, R.K.H. Singh, T. Swu, W.R. Devi and C.H.B. Singh, *J. Coord. Chem.*, **67**, 891 (2014); https://doi.org/10.1080/00958972.2014.902449
36. W.J. Geary, *Coord. Chem. Rev.*, **7**, 81 (1971); https://doi.org/10.1016/S0010-8545(00)80009-0
37. D. Basumatary, R.A. Lal and A. Kumar, *J. Mol. Struct.*, **1092**, 122 (2015); https://doi.org/10.1016/j.molstruc.2015.02.070
38. E.B. Seena, N. Mathew, M. Kuriakose and M.R.P. Kurup, *Polyhedron*, **27**, 1455 (2008); https://doi.org/10.1016/j.poly.2008.01.020
39. H. Zafar, A. Kareem, A. Sherwani, O. Mohammad, M.A. Ansari, H.M. Khan and T.A. Khan, *J. Photochem. Photobiol. B*, **142**, 8 (2015); https://doi.org/10.1016/j.jphotobiol.2014.10.004
40. Y. Jadegoud, O.B. Ijare, B.S. Somashekar, G.A. Nagana Gowda and B.H.M. Mruthyunjayaswamy, *J. Coord. Chem.*, **61**, 508 (2008); https://doi.org/10.1080/00958970701362523
41. J.-N. Li, *Inorg. Nano-Met. Chem.*, **43**, 832 (2013); https://doi.org/10.1080/15533174.2012.750344
42. Z.A. Taha, A.A.M. Ajlouni, Kh.A. Al-Hassan, A.K. Hijazi and A.B. Faiq, *Spectrochim. Acta A Mol. Biomol. Spectrosc.*, **81**, 317 (2011); https://doi.org/10.1016/j.saa.2011.06.018
43. M.L. Sundararajan, T. Jeyakumar, J. Anandakumaran and B. Karpanai Selvan, *Spectrochim. Acta A Mol. Biomol. Spectrosc.*, **131**, 82 (2014); https://doi.org/10.1016/j.saa.2014.04.055
44. K.M. Raj, B. Vivekanand, G.Y. Nagesh and B.H.M. Mruthyunjayaswamy, *J. Mol. Struct.*, **1059**, 280 (2014); https://doi.org/10.1016/j.molstruc.2013.12.010
45. G. Jia, A.L. Rheingold, B.S. Haggerty and D.W. Meek, *Inorg. Chem.*, **31**, 900 (1992); https://doi.org/10.1021/ic00031a036
46. C.D. Stewart, M. Pedraza, H. Arman, H.J. Fan, E.L. Schilling, B. Szpoganicz and G.T. Musie, *J. Inorg. Biochem.*, **149**, 25 (2015); https://doi.org/10.1016/j.jinorgbio.2015.04.012
47. E. Shurdha, C.E. Moore, A.L. Rheingold, S.H. Lapidus, P.W. Stephens, A.M. Arif and J.S. Miller, *Inorg. Chem.*, **52**, 10583 (2013); https://doi.org/10.1021/ic401558f
48. H.C. Fang, Y.Y. Ge, H.Y. Jia, S.S. Li, F. Sun, L.G. Zhang and Y.P. Cai, *CrystEngComm*, **13**, 67 (2011); https://doi.org/10.1039/C0CE00485E
49. N.F. Curtis and Y.M. Curtis, *Inorg. Chem.*, **4**, 804 (1965); https://doi.org/10.1021/ic50028a007
50. S. Gupta, B.K. Paul, A.K. Barik, T.N. Mandal, S. Roy, N. Guchhait, R.J. Butcher and S.K. Kar, *Polyhedron*, **28**, 3577 (2009); https://doi.org/10.1016/j.poly.2009.07.053
51. H. Hosseini-Monfared, R. Bikas, J. Sanchiz, T. Lis, M. Siczek, J. Tucek, R. Zboril and P. Mayer, *Polyhedron*, **61**, 45 (2013); https://doi.org/10.1016/j.poly.2013.05.033
52. S. Roy, T.N. Mandal, K. Das, R.J. Butcher, A.L. Rheingold and S.K. Kar, *J. Coord. Chem.*, **63**, 2146 (2010); https://doi.org/10.1080/00958972.2010.499457
53. S.A. Abdel-Latif, H.B. Hassib and Y.M. Issa, *Spectrochim. Acta A Mol. Biomol. Spectrosc.*, **67**, 950 (2007); https://doi.org/10.1016/j.saa.2006.09.013
54. D.N. Sathyanarayana, Electronic Absorption Spectroscopy and Related Technique, Universities Press India Limited, Edn.: 1, p. 284 (2001).
55. A.B.P. Lever and S.M. Nelson, *J. Chem. Soc. A*, 859 (1966); https://doi.org/10.1039/j19660000859
56. S.B. Kalia, K. Lumba, G. Kaushal and M. Sharma, *Indian J. Chem.*, **46A**, 1233 (2007).
57. J.P. Barbier, A. El Biyyadh, C. Kappenstein, N.D. Mabiala and R.P. Hugel, *Inorg. Chem.*, **24**, 3615 (1985); https://doi.org/10.1021/ic00216a028
58. S.A. Carabineiro, L.C. Silva, P.T. Gomes, L.C.J. Pereira, L.F. Veiros, S.I. Pascu, M.T. Duarte, S. Namorado and R.T. Henriques, *Inorg. Chem.*, **46**, 6880 (2007); https://doi.org/10.1021/ic062125w
59. R.L. Dutta and A. Syamal, Elements of Magnetochemistry, Affiliated East-West Press Private Limited, Edn.: 2, p. 103 (1993).
60. S.G. Sreerama, D. Shyamraj, S. Pal and S. Pal, *Indian J. Chem.*, **42A**, 2352 (2003).
61. A. Kulkarni, P.G. Avaji, G.B. Bagihalli, S.A. Patil and P.S. Badami, *J. Coord. Chem.*, **62**, 481 (2009); https://doi.org/10.1080/00958970802226387
62. A.B.P. Lever, Inorganic Electronic Spectroscopy, Elsevier Science, Amsterdam, Netherlands, Edn.: 2 (1984).
63. A.N. Kursunlu, E. Guler, F. Sevgi and B. Ozkalp, *J. Mol. Struct.*, **1048**, 476 (2013); https://doi.org/10.1016/j.molstruc.2013.06.017
64. R. Selwin Joseyphus and M. Sivasankaran Nair, *Arab. J. Chem.*, **3**, 195 (2010); https://doi.org/10.1016/j.arabjc.2010.05.001
65. B. Bleaney and R.S. Rubins, *Proc. Phys. Soc. Lond.*, **77**, 103 (1961); https://doi.org/10.1088/0370-1328/77/1/312
66. S. Chandra and L.K. Gupta, *Spectrochim. Acta A Mol. Biomol. Spectrosc.*, **61**, 2549 (2005); https://doi.org/10.1016/j.saa.2004.08.028
67. D. Kivelson and R. Neiman, *J. Chem. Phys.*, **35**, 149 (1961); https://doi.org/10.1063/1.1731880
68. P. Kavitha, M. Saritha and K. Laxma Reddy, *Spectrochim. Acta A Mol. Biomol. Spectrosc.*, **102**, 159 (2013); https://doi.org/10.1016/j.saa.2012.10.037
69. Ramina, R.B. Singh, O. U-wang, T.S. Singh and T.T. Jamir, *Asian J. Chem.*, **32**, 1667 (2020); https://doi.org/10.14233/ajchem.2020.22615
70. R.K. Gupta, G. Sharma, R. Pandey, A. Kumar, B. Koch, P.-Z. Li, Q. Xu and D.S. Pandey, *Inorg. Chem.*, **52**, 13984 (2013); https://doi.org/10.1021/ic401662d
71. K. Singh, P. Srivastava and A.K. Patra, *Inorg. Chim. Acta*, **451**, 73 (2016); https://doi.org/10.1016/j.ica.2016.07.003
72. B.J.M.L. Ferreira, P. Brandão, M. Meireles, F. Martel, A. Correia-Branco, D.M. Fernandes, T.M. Santos and V. Félix, *J. Inorg. Biochem.*, **161**, 9 (2016); https://doi.org/10.1016/j.jinorgbio.2016.04.026
73. F. Arjmand and M. Aziz, *Eur. J. Med. Chem.*, **44**, 834 (2009); https://doi.org/10.1016/j.ejmech.2008.05.006
74. H. Wu, J. Yuan, Y. Bai, H. Wang, G. Pan and J. Kong, *J. Photochem. Photobiol. B*, **116**, 13 (2012); https://doi.org/10.1016/j.jphotobiol.2012.07.005

75. M. Zampakou, N. Rizeq, V. Tangoulis, A.N. Papadopoulos, F. Perdih, I. Turel and G. Psomas, *Inorg. Chem.*, **53**, 2040 (2014); https://doi.org/10.1021/ic4025487
76. Y.-M. Sun, F.-Y. Dong, D.-Q. Wang and Y.-T. Li, *J. Braz. Chem. Soc.*, **22**, 1089 (2011); https://doi.org/10.1590/S0103-50532011000600013
77. Y. Li, Z. Yang, M. Zhou, Y. Li, J. He, X. Wang and Z. Lin, *RSC Adv.*, **7**, 41527 (2017); https://doi.org/10.1039/C7RA05504H
78. P. Zhao, S. Zhai, J. Dong, L. Gao, X. Liu, L. Wang, J. Kong and L. Li, *Bioinorg. Chem. Appl.*, **847**, 8152 (2018); https://doi.org/10.1155/2018/8478152
79. Q. Wei, J. Dong, P. Zhao, M. Li, F. Cheng, J. Kong and L. Li, *J. Photochem. Photobiol. B*, **161**, 355 (2016); https://doi.org/10.1016/j.jphotobiol.2016.03.053
80. H. Farrokhpour, H. Hadadzadeh, F. Darabi, F. Abyar, H.A. Rudbari and T. Ahmadi-Bagheri, *RSC Adv.*, **4**, 35390 (2014); https://doi.org/10.1039/C4RA04634J
81. N. Shahabadi, M. Mahdavi, A.A. Taherpour and F. Ghasemhezaveh, *J. Coord. Chem.*, **70**, 2589 (2017); https://doi.org/10.1080/00958972.2017.1363890
82. M.-J. Niu, Z. Li, G.-L. Chang, X.-J. Kong, M. Hong and Q. Zhang, *PLoS One*, **10**, e0130922 (2015); https://doi.org/10.1371/journal.pone.0130922
83. M. Ulusoy, H. Karabiyik, R. Kilincarslan, M. Aygun, B. Cetinkaya and S. Garcia-Granda, *Struct. Chem.*, **19**, 749 (2008); https://doi.org/10.1007/s11224-008-9358-z
84. M. Kuate, M.A. Conde, E.N. Mainsah, A.G. Paboudam, F.M.M. Tchieno, K.I.Y. Ketchemen, I.T. Kenfack and P.T. Ndifon, *J. Chem.*, **523**, 8501 (2020); https://doi.org/10.1155/2020/5238501
85. A. Gubendran, M.P. Kesavan, S. Ayyanaar, L. Mitu, P. Athappan and J. Rajesh, *Spectrochim. Acta A Mol. Biomol. Spectrosc.*, **181**, 39 (2017); https://doi.org/10.1016/j.saa.2017.03.031
86. I. Yousuf and F. Arjmand, *J. Photochem. Photobiol. B*, **164**, 83 (2016); https://doi.org/10.1016/j.jphotobiol.2016.09.016